Check for updates

Fe-Based metal–organic frameworks as functional materials for battery applications

Qingyun Yang,[a,b] Yanjin Liu,[a,b] Hong Ou,[b] Xueyi Li,[b] Xiaoming Lin, [ID] *[a,b] Akif Zeb [ID] [b] and Lei Hu [ID] *[a]

Metal–organic frameworks (MOFs), as a kind of organic–inorganic porous material with a high surface area, high porosity and versatile functionalities, have attracted significant research interest in the field of batteries in recent years. Among many MOF materials, Fe-based MOFs have many advantages, such as low toxicity, low cost, diverse structure types and preferable stability, which have splendid potential in practical applications. To further understand the contribution of Fe-based MOFs in battery application, we mainly review the applications of pristine Fe-MOFs in lithium-ion batteries, sodium-ion batteries, potassium-ion batteries, metal–air batteries and lithium–sulfur batteries in detail. Their electrochemical properties as cathodes, anodes and electrocatalysts are discussed and compared from the aspects of synthesis methods, reaction conditions and additives, which is expected to provide beneficial information and new perspectives for the application of Fe-MOFs as battery materials towards high electrochemical performance. Finally, through careful reflection on the research progress, we summarize the existing problems of Fe-MOFs and provide an outlook.

[a]*Anhui Laboratory of Functional Coordinated Complexes for Materials Chemistry and Application, School of Chemical and Environmental Engineering, Anhui Polytechnic University, Wuhu 241000, P.R. China. E-mail: hulei@ahpu.edu.cn*
[b]*Guangzhou Key Laboratory of Materials for Energy Conversion and Storage, Key Laboratory of Theoretical Chemistry of Environment, Ministry of Education, School of Chemistry, South China Normal University, Guangzhou 510006, P.R. China. E-mail: linxm@scnu.edu.cn*

1. Introduction

Nowadays, the energy problem is a non-negligible problem faced by mankind. Specifically, the global demand for energy is growing, but 80% of the world's total energy is currently produced by fossil fuels, which will not only cause the diffusion of pollutants in the atmosphere, but also have some negative effects on climate change and human health.[1] Due to the

Qingyun Yang will obtain her B.S. degree from South China Normal University and pursue her M.S. degree in 2022. She joined the group of Prof. Lin in 2018. Her research interests focus on physical chemistry and the applications of metal–organic frameworks and their derivatives in lithium-ion batteries.

Qingyun Yang

Xiaoming Lin received his M.S. degree in 2009 from South China Normal University and Ph.D. in 2012 from Sun Yat-Sen University, China. He joined the Department of Chemistry, South China Normal University, in 2013 and was promoted to Associate Professor in 2016. After working for one year as a visiting scholar at the University of Science and Technology of China, he worked as a postdoctoral fellow at South China University of Technology and EVE Energy Co., Ltd. His group aims to create unique metal–organic frameworks (MOFs) and their derivatives for electrochemical energy storage and conversion.

Xiaoming Lin

This journal is © the Partner Organisations 2022

Inorg. Chem. Front., 2022, **9**, 827–844 | 827

exhaustion of fossil energy and the deterioration of the environment, it is necessary to develop environmentally friendly and sustainable energy sources such as wind and solar energy.[2–4] However, the generation of these energy sources is intermittent, and it is necessary to combine them with energy storage devices that are stable, efficient, safe and capable of delivering massive amounts of clean electricity.[5] Therefore, the search for the next generation of energy-storage devices with high power density and energy density is receiving intensive attention from both fundamental research and industry, resulting in a certain necessity to develop new materials.

Metal–organic frameworks (MOFs) are a kind of organic–inorganic porous material, which are formed by the coordination between organic ligands and inorganic metal ions or clusters. Due to high porosity, large specific surface area and redox active metal vertices, MOFs have been widely used in the fields of energy storage, gas storage, hydrocarbon storage, semiconductors, drug delivery and catalysis. In the fields of energy storage, MOFs often serve as a kind of potential new electrode material.[6–9] Firstly, high porosity and large specific surface area are beneficial for interfacial charge transport, which provides short diffusion paths for ions.[10] Secondly, MOFs have high thermal stability compared with pure organic materials, and the separation of metal ions at atomic scale allows metal ions to be utilized more efficiently. Thirdly, by selecting suitable metal centers and organic ligands, the structural properties of the MOFs can be tuned and the operating potential can be adjusted to reduce the risk of an exothermic reaction with the electrolyte, which is significant for high-power batteries.[11–14]

The key to battery research lies in electrode materials. Transition metal compounds with many advantages (high theoretical capacity, low cost, environmental friendliness, and safety) have been widely favored by researchers. As a typical transition metal, iron-based materials have been proved to be excellent electrode materials, mainly due to iron's low price, rich sources, accounting for 5.1% of the crust quality, ranking fourth in the distribution of elements in the world, and high theoretical capacity. More importantly, a typical feature of Fe-MOFs is the Fe unsaturated metal centers (UMCs),[15] the strong Fe–O coordination bond between unsaturated metal centers (Fe(III)) and O atoms in organic ligands owing to the high energy density of Fe UMCs, which is consistent with Pearson's acid/base theory, leading to the favorable properties and chemical versatility of Fe-MOFs, such as high safety, high service life, support for rapid charging and a wide range of operating temperatures.[16–22] As early as 2007, a mixed-valence Fe-MOF, namely $[Fe^{III}(OH)_{0.8}F_{0.2}(O_2CC_6H_4CO_2)]\cdot H_2O$ (MIL-53 (Fe)·H_2O), was for the first time directly used as a cathode material for lithium-ion batteries, which is the first example of reversible electrochemical lithium insertion in the Fe-MOF system.[23] Unfortunately, this material had a poor capacity of about 70 mA h g^{-1}. After that, other Fe-MOFs have been continuously developed and reported, such as MIL-68(Fe),[24] MIL-88B(Fe),[25] MIL-101(Fe),[26] etc., which showed promising performance in battery applications. Compared with traditional porous materials, Fe-MOFs perform better in a wide variety of applications. For instance, the internal pore environment and pore size were effectively controlled by the flexibility of Fe-MOFs, which further promoted the access of guest molecules.

Hence, this article will present an up-to-date and detailed review in regard to the applications of Fe-based metal–organic frameworks in the field of electrochemical energy storage (Fig. 1), such as lithium-ion batteries (LIBs), sodium-ion batteries (SIBs), potassium-ion batteries (PIBs), metal–air batteries (MABs) and lithium–sulfur batteries (LSBs). Finally, through careful reflection on the research progress, we summarize the existing problems of Fe-MOFs and provide an outlook.

Akif Zeb received his B.S. degree from Hazara University (2007), M.S. degrees in inorganic and analytical chemistry (2011) and in materials and surface engineering (2014) from Quaid-i-Azam University and the National University of Sciences and Technology, Pakistan, respectively. He received his Ph.D. in 2018 in inorganic chemistry from the University of Science and Technology of China. Currently, he is working as a postdoctoral fellow with Prof. Xiaoming Lin at South China Normal University. His research is focused on the design and development of new nanomaterials for energy storage and conversion, heterogeneous catalysis and biomimetics.

Akif Zeb

Lei Hu received his M.S. degree in applied chemistry from South China Normal University and Ph.D. in physical chemistry from Sun Yat-sen University. He joined the Department of Chemical and Environmental Engineering, Anhui Polytechnic University in 2020. His research mainly focuses on electrochemical energy conversion and storage materials, especially in the fields of water splitting and lithium-ion batteries.
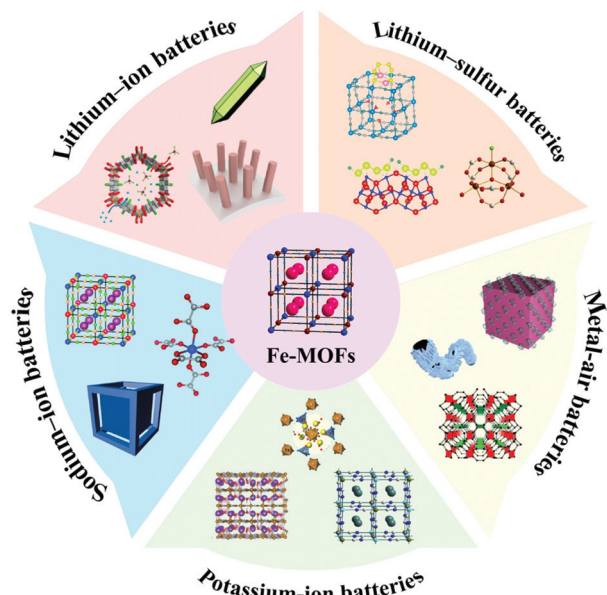
Lei Hu

Fig. 1 Fe-MOFs for battery applications.[27–42]

2. Fe-Based MOFs for battery applications

2.1. Lithium-ion batteries

A lithium-ion battery (LIB) is the key to the rapid upgrading of portable electronic devices and the development of newly emerging large-scale applications (electric vehicles and grid storage) because of its high energy density, power density and long cycling life.[43] In order to further improve the energy density and power density of LIBs, it is necessary to develop new MOF materials with better performance, lower cost and a simpler synthesis method.[44,45] Table 1 summarizes the electrochemical performances of various Fe-based MOFs for LIBs.

As early as 2007, Férey et al. proposed to use MOFs based on early transition metals with lower occupation of the 3d-electron orbital and higher oxidation states.[23] They synthesized the MIL-53(Fe) series [$Fe^{III}OH(bdc)$] (MIL = materials of Institute Lavoisier, bdc = 1,4-benzenedicarboxylate), which improved the stability of M–O bond, and achieved long-range electron delocalization through the stabilization of mixed-valence states related to a double exchange mechanism. Unfortunately, MIL-53(Fe) didn't show the expected electrochemical performance because the carboxylic group of the terephthalate ligands were not activated, which was caused by the thick solid electrolyte SEI layer and poor conductivity.[46] It is worth mentioning that the synthesis process of MIL-53(Fe) requires HF, which limited its potential as a large scale grid storage battery material. Later, Shin et al. prepared MIL-101(Fe) as a candidate electrode in order to avoid using HF (Fig. 2a).[26] Nevertheless, the relaxation of Fe^{2+} to Fe^{3+} led to the irreversible accumulation of Li^+ in MIL-101(Fe), resulting in the rapid decay of capacity.

In order to achieve sufficient specific capacity, the redox activity of organic linkers must be achievable at high potential. Ziebel et al. reported two iron-semiquinoid frameworks with the formula of $(H_2NMe_2)_2Fe_2(Cl_2 dhbq)_3$ ($Cl_2 dhbq^{n-}$ = deprotonated 2,5-dichloro-3,6-dihydroxybenzoquinone) that combined metal- and ligand-centered redox activity to achieve considerably high lithium storage capacity at high current density, whose energy densities were up to 533 W h kg^{-1}. The framework based on 2,5-dihydroxybenzoquinone (H_2 dhbq) manifested d–π conjugation that contributed to the charge hopping between mixed-valent ligands centers.[27] Recently, Li et al. selected 1,1′-dicarboxyferrocene (DFc) as the primary material to coordinate with the Fe^{3+} cation to prepare nanosized $Fe_2(DFc)_3$ with high redox potential.[47] They found that the discharge capacity could be attributed to the reduction of Fe^{3+} and the contribution of conductive additives (Ketjenblack (KB) and carbon nanotubes (CNTs), 15 wt% each). The as-fabricated

Table 1 Fe-MOF based electrode materials for LIBs

Fe-MOF	Electrode	Vs. Li/Li$^+$	Initial DC/CC (mA h g^{-1})	RC/rate (C or mA g^{-1})	Cycle number	Ref.
[$Fe_3O(BDC)_3(H_2O)_2(NO_3)$]$_n$	Anode	0.005–3.0	1507.4/949.9	744.5/60	400	6
MIL-53(Fe)	Cathode	1.5–3.5	77/80	71/0.025 C	50	23
MIL-68(Fe)	Cathode	1.5–3.5	—/—	30/0.1 C	3	24
MIL-88B(Fe)	Anode	0.01–3.0	1275.4/585.5	680/200	500	25
MIL-101(Fe)	Cathode	2.0–3.5	66.8/84.6	39.9/0.025 C	5	26
$(H_2NMe_2)_2Fe_2(Cl_2 dhbq)_3$	Cathode	1.8–4.2	167/—	147/40	50	27
CPO-27@250	Anode	0.1–3.0	—/490	456/1000	500	28
MIL-88A@PMo$_{12}$	Anode	0.01–3.0	1451.60/671.66	1062.1/200	100	29
$Fe_2(DFc)_3$	Cathode	2.0–4.5	240/—	130/50	100	47
MIL-53(Fe)@RGO	Anode	0.01–3.0	—/—	550/100	100	48
PCN-600	Anode	0–3.0	—/885	1580/100	140	53
PMo$_{10}$V$_2$-ILs@MIL-100	Anode	0.01–3.0	1665.5/1114.9	1258.5/100	100	62
mFeP-NM	Anode	0.01–3.0	—/314	458/200	160	63
MIL-116(Fe)	Cathode	2.0–4.4	—/—	100/—	60	64
K$_{0.07}$Fe[Co(CN)$_6$]$_{0.89}$·7.5H$_2$O	Cathode	2.2–4.5	136/—	150/100	40	65
Fe-BTC	Anode	0.01–3.0	1765.5/683.2	1021.5/100	100	66
Fe-MOF	Anode	0.01–3.0	—/600	825/250	100	67

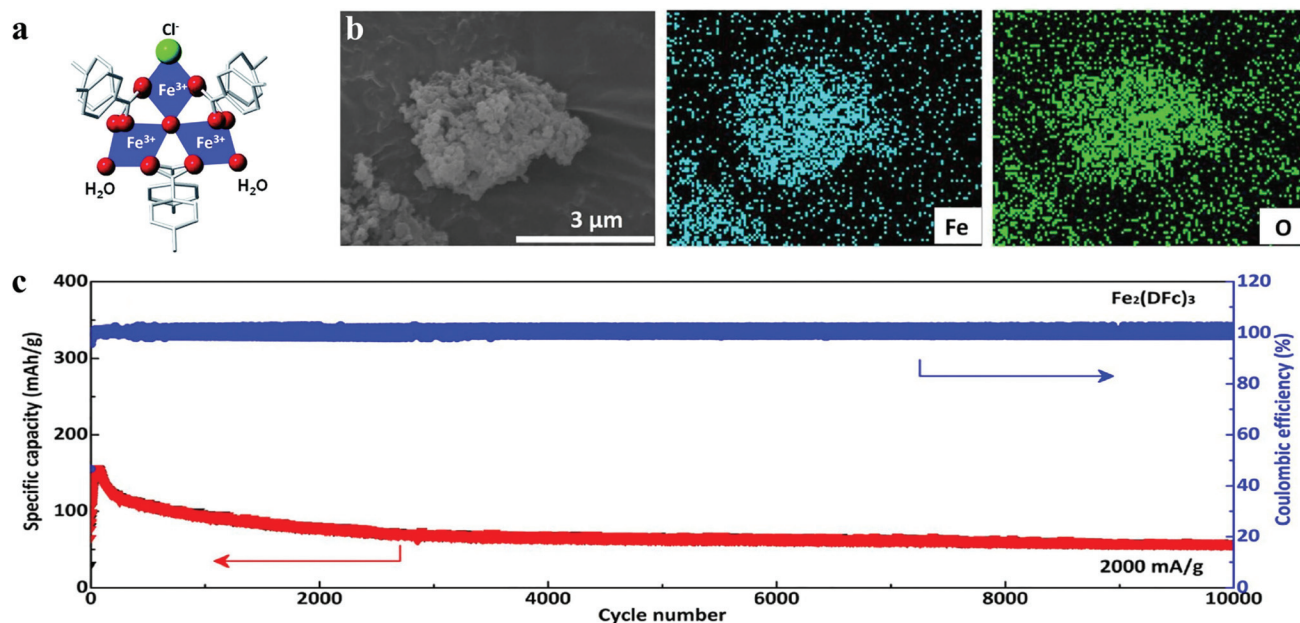DC: discharge capacity, CC: charge capacity, RC: reversible capacity.

Fig. 2 (a) Structure of MIL-101(Fe).[26] (b) EDS mapping of $Fe_2(DFc)_3$.[47] (c) Long-cycle profiles under a current density of 2000 mA g^{-1} of $Fe_2(DFc)_3$.

batteries manifested eximious electrochemical performance with a high operation potential of 3.55 V (*vs.* Li$^+$/Li), whose capacity was also retained at 85% after 10 000 cycles at 2000 mA g^{-1} (Fig. 2b and c).

In addition to the above-mentioned cathode application of Fe-MOF materials, Fe-MOFs can also be applied as an anode material for LIBs. For instance, Shen *et al.* synthesized a kind of iron based MOF polyhedral nanorod Fe-MIL-88B ([Fe$_3$O (BDC)$_3$(H$_2$O)$_2$(NO$_3$)]$_n$) structure.[6] The *ex situ* XRD patterns of the Fe-MIL-88B electrode showed that all the diffraction peaks appear in the initial charge/discharge and re-discharged electrodes (Fig. 3a and b), indicating that the open framework structures were well maintained during Li$^+$ ion insertion/deinsertion. The π–π interactions of conjugated carboxylates reduced the dissolution of Fe-MIL-88B in organic electrolytes, resulting in excellent cycling stability. Subsequently, to improve the conductivity of the material and reduce the direct contact between the material and electrolyte, the addition of reduced graphene oxide (RGO) activated carboxylic groups, thus led to the generation of MIL-53(Fe)@RGO, exhibiting better electrochemical performance (Fig. 3d–g).[48]

Some MOFs can accommodate a large number of Li$^+$ ions, but they suffer from side reactions during lithiation/delithiation, low conductivity, and slow ion diffusion kinetics. MOFs can generate metal oxides and carbon through thermal treatment above 400 °C. Although the conductivity is improved, it will destroy the immanent organic–inorganic hybrid structure.[49–51] However, under suitable low temperature annealing conditions, both the weight loss, structural damage and energy consumption are less. Simultaneously, it can remove the solvent molecules in MOF channels so as to reduce the occurrence of side reactions, increase the diffusion coeffi-

cient of Li$^+$ ions, and further improve the lithium storage performance.[52] For instance, Zhou and co-workers designed three-dimensional nanorod arrays as an efficient lithium anode by combining the multi-component CPO-27 (MOF compounds based on 2,5-dihydroxyterephthalic acid) composed of iron, cobalt and nickel with low-temperature heating (Fig. 3h and i).[28] In this structure, the interaction between various metal components boosts the electronic delocalization in CPO-27, pursuantly increasing the electronic conductivity. The design of a three-dimensional self-supporting array structure considerably reduced the transport pathways of ions and electrons. The results showed that when the thermal treatment temperature was 250 °C, CPO-27@250 showed the best comprehensive performance, its amorphous state might promote ion diffusion, and the surface contribution rate was the highest. CPO-27@250 affords a high reversible capacity of 834 mA h g^{-1} at 50 mA g^{-1}, and sustains 93% of the capacity over 500 cycles at 1000 mA g^{-1}.

Besides the materials of the polycarboxylic acid organic ligand, many rigid organic ligands are also used for the synthesis of iron-based organic framework materials. In 2018, the iron porphyrin-based metal–organic framework (namely PCN-600) was firstly used as anodic electrode for lithium-ion batteries.[53] The 3D mesoporous PCN-600 samples prepared on the basis of [Fe$_3$O(OOCCH$_3$)$_6$OH]$_2$H$_2$O exhibited unprecedented high capacity as MOF anode materials on account of the synergistic effect of the Fe cluster center and porphyrinic ligands. The PCN-600 anode delivered a reversible capacity of 1300 mA h g^{-1} at 400 mA g^{-1}, and retained 1580 mA h g^{-1} after 140 cycles at 100 mA g^{-1}. As a traditional organic transition metal complex, ferrocene contains one central iron cation (Fe^{2+}) and two cyclopentadienyl anions, which can
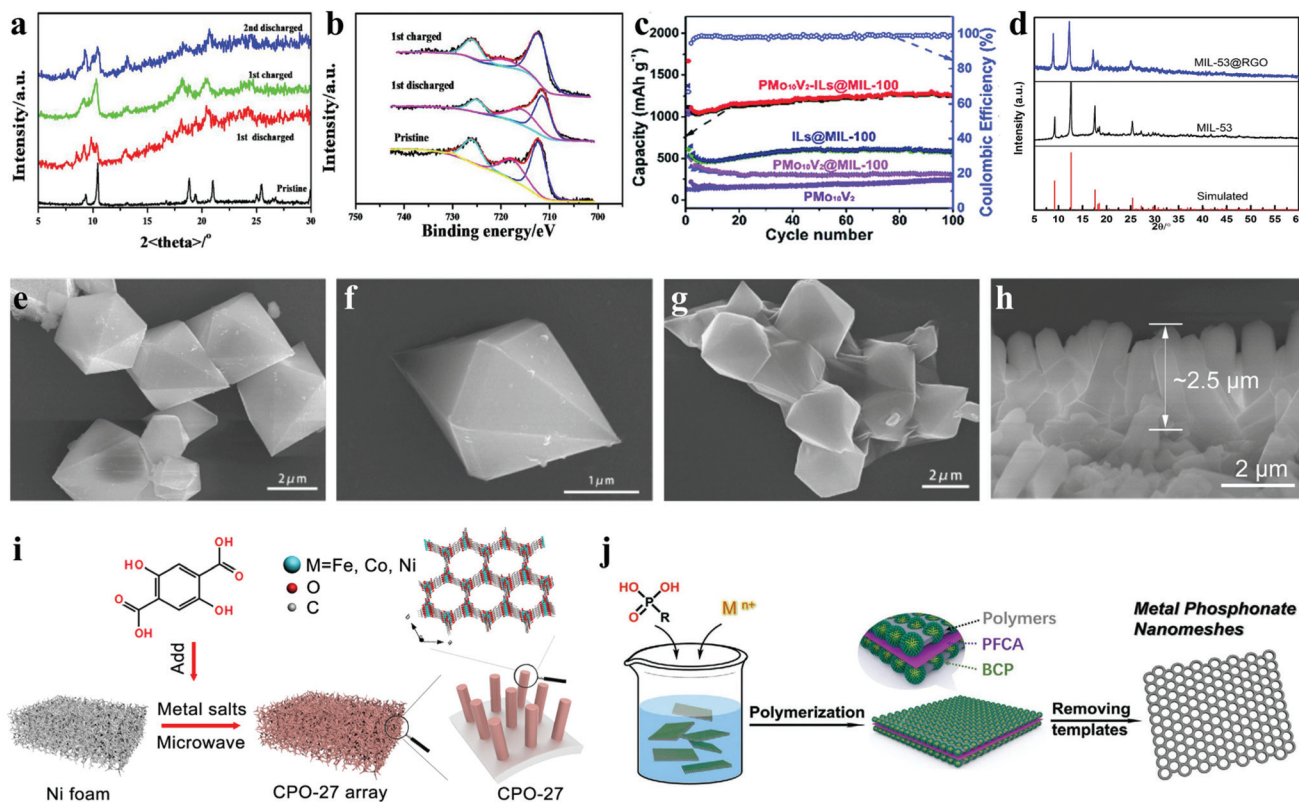
830 | *Inorg. Chem. Front.*, 2022, **9**, 827–844

This journal is © the Partner Organisations 2022

Fig. 3 *Ex situ* characterization of the Fe-MIL-88B nanorod electrode at different charge−discharge stages: (a) XRD pattern variations; and variations in the Fe 2p XPS core spectra.[6] (c) Charge/discharge capacity and coulombic efficiency of $PMo_{10}V_2$, $PMo_{10}V_2@MIL-100$, ILs@MIL-100 and $PMo_{10}V_2$-ILs@MIL-100 crystals at 0.1 A g^{-1}.[29] (d) XRD patterns of the MIL-53(Fe) and MIL-53(Fe)@RGO samples; and SEM images of (e and f) MIL-53 (Fe) and (g) MIL-53(Fe)@RGO.[48] (h) SEM image of CPO-27@250 and (i) schematic illustration of the preparation of CPO-27 arrays.[28] (j) Scheme for the synthesis of mesoporous metal−organic nanomeshes.[63]

perform reversible redox reactions and be used as an efficient and stable cathode for LIBs.[54,55] In order to overcome the high solubility of ferrocene in organic solvents and electrolytes, introducing electron-withdrawing groups can make the materials obtain lower solubility and higher redox potential to achieve higher capacity.[56,57]

In particular, as early transition metal anionic clusters, polyoxometalates (POMS) are known as "electron sponges", which have reversible multi-electron redox properties and high capability to accept a huge number of electrons.[58–61] In 2018, Zhang *et al.* reported $PMo_{10}V_2$-ILs@MIL-100,[62] in which $PMo_{10}V_2$ is inserted into MIL-100 cages as a bridge, ionic liquids (ILs) can be easily dispersed into MIL-100 mesoporous cages with enhanced conductivity. Therefore, it showed a surprisingly high initial discharge capacity of 1665.5 mA h g^{-1} at 100 mA g^{-1}, and retained 1258.5 mA h g^{-1} after 100 cycles (Fig. 3c). In 2020, Zhao *et al.* reported MIL-88A@PMo_{12}.[29] During the synthesis process, phosphomolybdic acid leads to the low pH of the reaction system, which was not conducive to the formation of MIL-88A with high crystallinity. Therefore, MIL-88A@PMo_{12} with an amorphous structure was obtained with a smooth surface and no aggregation. It is worth mentioning that $PMo_{10}V_2$ cluster's reversible redox properties and water solubility were stronger than those of the PMo_{12} cluster

due to the reason that the V atom in the $PMo_{10}V_2$ cluster can increase the redox potential of the first electron transfer reaction. Later, Ai's group used metal phosphate to synthesize mesoporous ferric phytate nanomeshes (mFeP-NMs), the detailed synthesis procedure of mFeP-NMs is shown in Fig. 3j.[63] Thanks to the unique two-dimensional ultrathin monolayer nanostructures (∼9 nm thickness), it had preferable charge storage and ion transport properties. Compared with carboxylates, metal phosphonates show higher thermal and chemical stability because the affinity of metal ions is strong. This work provided a new template for the synthesis of mesoporous metal–organic nanomeshes.

2.2. Sodium-ion batteries

In the past few decades, LIBs have played a dominant role in the competitive field of energy storage systems.[68] However, due to the limited resources of lithium on Earth, the demand for alternative systems with comparable performance to LIBs has promoted the research and exploitation of different materials and composites with other more abundant alkaline metals such as sodium or potassium.[69,70] Because of low cost, low toxicity and abundance of sodium resources, sodium-ion batteries (SIBs) have attracted increasing interest.[71,72] Table 2 lists the

This journal is © the Partner Organisations 2022

Inorg. Chem. Front., 2022, **9**, 827–844 | 831

Table 2 Fe-MOF based electrode materials for SIBs

Fe-MOF	Vs. Na/Na$^+$	Initial DC/CC (mA h g^{-1})	RC/rate (C or mA g^{-1})	Cycle number	Ref.
K$_4$Na$_2$[Fe(C$_2$O$_4$)$_2$]$_3$·2H$_2$O	1.6–4.0	49.5/54.5	45/0.02 C	10	30
FeFe(CN)$_6$/carbon	−0.4–0.6 (vs. SCE)	53/—	—/100	—	31
NiFe(II) PBA	2.0–4.0	57/—	51/100	500	32
FeFe(CN)$_6$	−0.8–1.2 (vs. Ag/AgCl)	96/—	90/700	400	77
PB/MoS$_2$	—	177/—	—/1000	—	80

DC: discharge capacity, CC: charge capacity, RC: reversible capacity.

electrochemical performances of various Fe-based MOFs for SIB electrode materials.

The oxalato-bridged networks continue to receive much attention, because the oxalato ligand has high degrees of freedom of the bridging modes, allowing a large variety of structures. Wang *et al.* prepared a new Fe-oxalato open framework K$_4$Na$_2$[Fe(C$_2$O$_4$)$_2$]$_3$·2H$_2$O for reversible Na$^+$ intercalation/extraction in 2014, which is the first discovery of the ion intercalation ability of an open frame composed of only oxalate bridges.[30] The Fe atom is coordinated octahedrally by O atoms from oxalato ligands that are crystallographically distinct, the crystal structure of K$_4$Na$_2$[Fe(C$_2$O$_4$)$_2$]$_3$·2H$_2$O is shown in Fig. 4a and b. In addition, in 2017, Chavez's team reported the feasibility of the Fe-MIL-100 as electrodes for aqueous SIBs.[73] However, the capacity of Fe-MIL-100 decreases rapidly in the cycle with poor reversibility, which may be due to the inability to access active sites reversibly for sodium intercalation. An oxalate ligand has the bridging mode with high degrees of freedom, and can be used as powerful ion intercalation electrode materials.[74,75]

Among numerous potential SIB electrode materials, Prussian blue (PB): A$_{2−x}$M$_a$[M$_b$(CN)$_6$]$_{1−y}$·zH$_2$O (A: alkali cations, M: metal ions) have attracted enormous attention, in which M$_b$ is usually a Fe atom, thus they are called hexacyanoferrates (HCF).[34] PB has a structural arrangement that allows Fe to be partially substituted by other transition metal ions (such as Co^{II}, Co^{III}, Cu^{II}, and Ni^{II}) in different oxidation states, forming Prussian blue analogs (PBAs).[76] As a promising cathode material for high rate aqueous SIBs, Yang *et al.* studied and compared the electrochemical performance of highly crystalline FeFe(CN)$_6$ in Na$^+$ aqueous solutions (Fig. 4c).[77] The electrochemical behavior of FeFe(CN)$_6$ in SIBs showed a capacity of 118 mA h g^{-1} at 400 mA g^{-1}, and retained 94% of the initial capacity after 400 cycles at 700 mA g^{-1} due to its good reversible redox reaction for insertion/extraction of Na ions. Besides, FeFe(CN)$_6$/carbon cloth has also been proved to
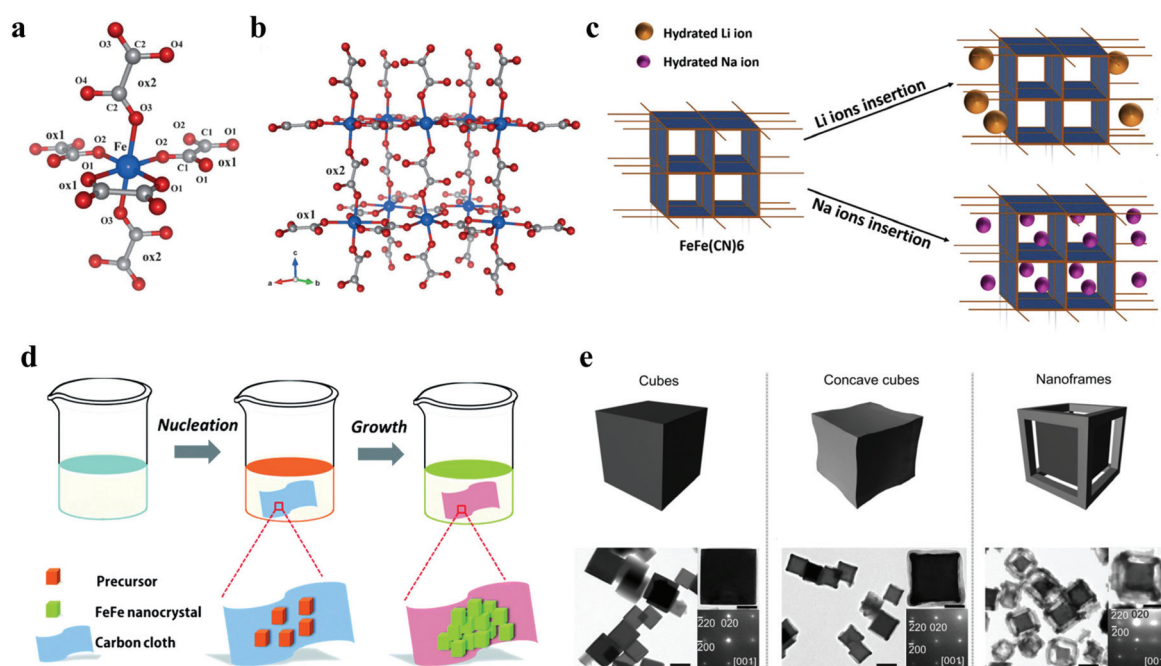

Fig. 4 Crystal structure of K$_4$Na$_2$[Fe(C$_2$O$_4$)$_2$]$_3$·2H$_2$O, with iron atoms shown in blue, carbon atoms in grey, and oxygen atoms in red, (a) coordination environment around Fe and (b) the 3D iron-oxalato framework.[30] (c) Schematic of Li and Na ion insertion for FeFe(CN)$_6$.[77] (d) Schematic illustration of the process used for the synthesis of FeFe(CN)$_6$/carbon cloth composites.[31] (e) Nanostructure evolution and TEM images of NiFe(II) PBA cubes, NiFe(II) PBA concave cubes and NiFe(II) PBA nanoframes.[32]

832 | *Inorg. Chem. Front.*, 2022, **9**, 827–844

This journal is © the Partner Organisations 2022

be suitable for aqueous SIBs (Fig. 4d).[31] However, the rapid capacity decay was observed through the rate performance test, which may be due to the corrosion of the electrode connecting wire in acidic solution. Furthermore, the crystal structure of $FeFe(CN)_6$ was gradually destroyed by rapid cation migration. In addition, as one of the most studied inorganic layered transition metal dichalcogenides (TMDCs), MoS_2 has been widely used in LIBs, SIBs, supercapacitors *etc.* for its excellent properties.[78,79] Morant-Giner *et al.* reported a simple method for preparing PB/MoS_2 based composites, which also provided a new way to combine other TMDCs with PBAs as energy storage composites.[80] As the materials of SIBs and PIBs, PB/MoS_2 showed excellent cycling stability, whose capacity retention was more than 97% after 10 000 cycles at 10 A g^{-1}.

Although PB and PBAs have the flexibility of cationic substitution in the crystal lattices, they can easily grow into large crystals. Monocrystalline nanoframes, as a kind of hollow nanostructure, porous on each face, are expected to be ideal candidate materials because they can provide a large contactable surface area and high crystallinity at the same time.[81,82] Zhang *et al.* prepared single crystal NiFe(II) PBA nanostructures by preferential etching.[30] Compared with the initial cubes, the nanoframes not only made the intercalation of Na^+ ions easier, but also significantly improved the rate performance and cycling stability (Fig. 4e). After 500 cycles at 100 mA g^{-1}, the capacity retention of the nanoframes was 90%, much higher than the 55% of the initial cubes.

2.3. Potassium-ion batteries

Except for LIBs and SIBs, potassium-ion batteries (PIBs) have also been receiving much interest recently. The most outstanding advantage is the exceptional negative potential: the standard potential of K^+/K (−2.88 V *vs.* the SHE) is 0.09 V lower than that of Li^+/Li (−2.79 V *vs.* the SHE) and 0.32 V lower than Na^+/Na (−2.56 V *vs.* the SHE) in organic solvent PC.[83]

Therefore, PIBs can obtain higher energy density and voltage operation than LIBs and SIBs. In addition, the charge density between K^+ (0.09 e $Å^{-3}$) is lower than Na^+ (0.23 e $Å^{-3}$), which makes K^+ have higher mobility in nonaqueous solution.[33] Table 3 presents the electrochemical performances of various Fe-based MOFs for KIBs.

Although some layered metal oxides (K_xMO_2) have been reported and cycle up to several hundred times, probably due to the larger ionic radius of K^+ (1.38 Å) than Li^+ (0.76 Å) and Na^+ (1.02 Å), some phosphate ($K_3V_2(PO_4)_3$) and layered K_xMO_2 materials are not satisfactory for K^+ extraction/insertion in the structure.[84,85] Fortunately, because of its large intrinsic interstitial cavities, facile preparation and low cost, Prussian blue and its analogues as cathode material for PIBs were widely reported.[34,86] Owing to the strong bonding between the carbon/nitrogen end of the cyanide ligand and the partially filled d-orbitals of Fe^{2+} and Fe^{3+} ions, pristine PB has a simple synthesis process and stable properties.[87] Unfortunately, it is not suitable for lithium-ion batteries, the research result of Imanishi *et al.* showed that the positive electrode with PB for a lithium rechargeable battery loses 30% capacity after only 10 cycles.[88,89] The stable PB film can participate in 10^7 reversible cycles of K^+ insertion/extraction, while the insertion/extraction of lithium ion destroys the lattice structure of the film, which makes its electrochemical activity decay in several cycles.[90,91] The crystal size is closely related to the material properties. He *et al.* explored the relationship between the crystallite size and performance of Prussian white, which showed that the ultrasmall $K_{1.7}Fe[Fe(CN)_6]_{0.9}$ crystallites offered the highest discharge capacity. Similarly, the aggregation of bulk synthesized Prussian blue inevitably leads to the limitation of K^+ mobility and the inhibition of potassium storage performance. To improve this situation, Qin *et al.* synthesized an ultrathin nanosheet-assembled hierarchical $K_{1.4}Fe_4[Fe(CN)_6]_3$ (PB-NSs) by a facile dissolution-recrystallization strategy, which provides

Table 3 Fe-MOF based electrode materials for PIBs

Fe-MOF	Vs. K/K$^+$	Initial DC/CC (mA h g^{-1})	RC/rate (C or mA g^{-1})	Cycle number	Ref.
$K_{1.88}Zn_{2.88}[Fe(CN)_6]_2(H_2O)_5$	3.4–4.15	55.6/64.9	—/0.1 C	100	33
$K_2Fe^{II}[Fe^{II}(CN)_6]\cdot 2H_2O$	0–1.2 (*vs.* Ag/AgCl)	120/140	115/200	100	34
$K_{0.3}Ti_{0.75}Fe_{0.25}[Fe(CN)_6]_{0.95}\cdot 2.8H_2O$	1.0–4.5	113/—	73.1/100	100	35
$K_{1.68}Fe_{1.09}Fe(CN)_6\cdot 2.1H_2O$	2.0–4.5	110.5/105.1	105/20	3	36
$K_{1.4}Fe_4[Fe(CN)_6]_3$	2.0–4.0	72/—	57.7/50	40	92
$KFe^{II}[Fe^{III}(CN)_6]$	2.0–4.5	118.7/—	111.3/10	100	93
$K_{1.49}Ni_{0.36}Co_{0.64}[Fe(CN)_6]_{0.91}\cdot 0.89H_2O$	2.0–4.5	86/—	75.9/20	300	94
$K_2Ni_{0.05}Fe_{0.95}Fe(CN)_6$	2.0–4.5	123.50/—	116.58/100	50	95
$K_{1.75}Mn[Fe(CN)_6]_{0.93}\cdot 0.16H_2O$	2.0–4.5	117/192	137/30	5	96
CNT/PB	−0.2–1.2 (*vs.* Ag/AgCl)	8.3/— (mA h cm^{-3})	6.1/2.5 (mA h cm^{-3})/μA	1000	99
$K_{1.85}Mn[Fe(CN)_6]_{0.98}\cdot 0.7H_2O/G$	2.0–4.5	108.8/—	103.2/5 C	500	100
MOF-235 + 20M	0.01–3.0	—	132/200	200	101
MOF-235 + 20G	0.01–3.0	—	180/200	200	102
KHCF@PPy	2.0–4.2	88.8/—	77.1/50	500	103
$K_{0.220}Fe[Fe(CN)_6]_{0.805}\cdot 4.01H_2O$	2.0–4.0	68.5/—	64/100	50	104
$K_{1.92}Fe[Fe(CN)_6]0.94\cdot 0.5H_2O$	2.0–4.3	—	133/0.1 C	200	105
$K_{1.93}Fe[Fe(CN)_6]_{0.97}\cdot 1.82H_2O$	−0.2–1.0 (*vs.* SCE)	100.1/—	88.2/1500	300	110
$K_{1.7}Fe[Fe(CN)_6]_{0.9}$	2.0–4.5	120/—	102/100	100	111

DC: discharge capacity, CC: charge capacity, RC: reversible capacity.

a new nanostructure strategy to improve the potassium storage performance of the intercalated electrode.[92] As confirmed by TEM, the thickness of this ultrathin nanosheets is about 10 nm (Fig. 5a–c). Thanks to the ultrathin nanosheet-assembled hierarchical structure, the diffusion path is shortened, more active sites are exposed, which results in higher specific capacity and lower polarization. Compared with the bulk samples (PB-NBs), we could find that PB-NSs showed more superior cycling performance (75.2% of initial capacity retained after 100 cycles) and rate performance (71 and 24.9 mA h g^{-1} at 50 and 600 mA g^{-1}), as shown in Fig. 5d. In addition, Chong's team reported a ferrous ferricyanide nanoparticle, $KFe^{II}[Fe^{III}(CN)_6]$ (KFFCN), as a cathode material for nonaqueous KIBs, which has a unique 3D open framework structure, nanoparticle morphology, two electron shuttle per formula unit and solid solution process, rather than phase transition for K$^+$ extraction/insertion (Fig. 5i).[93] *Ex situ* characterizations show that it can maintain reversible redox reactions and a stable structure in a long-term cycle. Therefore, KFFCN has an ultra-long cycle life of 1000 cycles and minimal capacity

fading at a current density of 100 mA g^{-1}. Hence, low-cost and excellent electrochemical performance make it promising for a large-scale electrical energy storage system.

Ternary materials provide a new way to improve the electrode performance by doping other transition metal ions such as nickel, manganese, zinc, titanium, *etc.* Ni doping can effectively improve the conductivity, causing crystallinity/orderliness changes, and have an influence on Fe and –C≡N– groups, including the motivation of Ni towards the C end connected Fe, and the effect of Ni on the electronic structure of the –C≡N– group.[94] For example, Huang *et al.* systematically studied the effect of Ni-doping on $K_2FeFe(CN)_6$, and found that doping with a suitable amount of Ni promoted/activated the redox reaction of C-coordination $Fe^{2+}C_6/Fe^{3+}C_6$ by changing the electronic state of Fe and boosting the diffusion of K ions during the charge and discharge process.[95] The optimal sample $K_2Ni_{0.05}Fe_{0.95}Fe(CN)_6$ showed excellent long cycling stability and a high initial capacity of 135 mA h g^{-1}. Particularly, the high-voltage plateau capacity increased from ~40 mA h g^{-1} to 53 mA h g^{-1}. As a cheap and environmentally
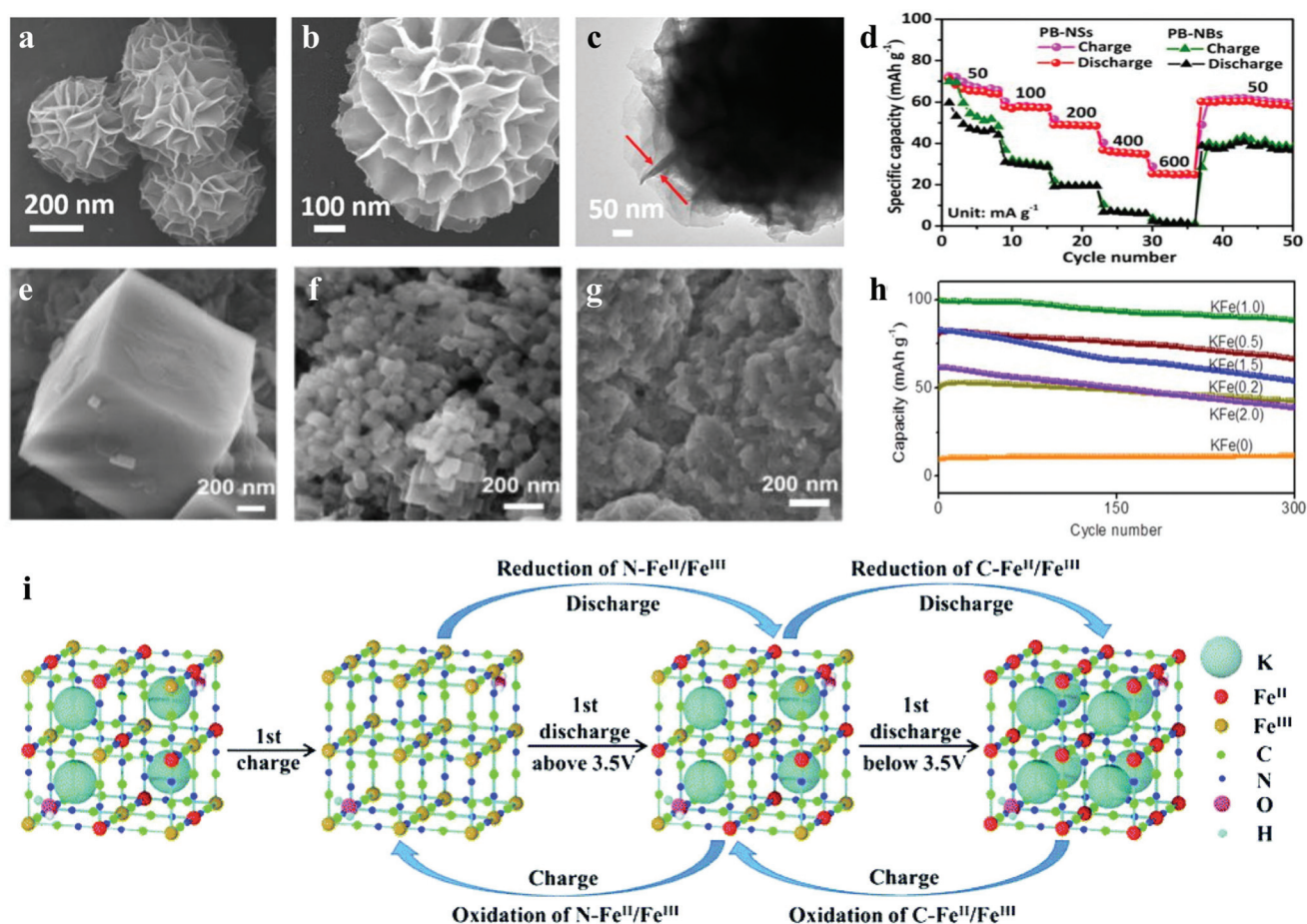

Fig. 5 Morphological characterization and evolution of PB-NSs by (a and b) SEM and (c) TEM images of PB-NSs and (d) the rate performances of PB-NSs and PB-NBs.[92] SEM images of (e) KFe(0), (f) KFe(1.0) and (g) KFe(2.0); and (h) cycling performances tested at 1500 mA g^{-1} (10 C) for all KFe samples.[110] (i) Schematic view of the K-ion extraction/insertion mechanism during the initial charge–discharge process and subsequent cycles for the KFFCN electrode.[93]

834 | *Inorg. Chem. Front.*, 2022, **9**, 827–844

This journal is © the Partner Organisations 2022

friendly transition metal, manganese doping is also considered to be a feasible way of improving electrode performance. In the $K_{1.75}Mn[Fe(CN)_6]_{0.93} \cdot 0.16H_2O$ (K-MnHCFe) prepared by Bie *et al.*, Mn and Fe atoms at octahedral sites are alternately arranged by the coordination bonds connecting nitrogen and carbon, respectively.[96] The open framework structure of MnN_6 and FeC_6 octahedra are bridged by cyanide ligands, which provides a large diffusion tunnel for K^+ at the interstitial sites. K-MnHCFe not only has a high reversible capacity of 141 mA h g^{-1} and high energy density of 536 W h kg^{-1}, which is equivalent to that of $LiCoO_2$ (~532 W h kg^{-1} *versus* Li), but also exhibits excellent rate performance and cycle performance. Besides, both zinc-doped $K_{1.88}Zn_{2.88}[Fe(CN)_6]_2(H_2O)_5$ [33] and titanium-doped $K_{0.3}Ti_{0.75}Fe_{0.25}[Fe(CN)_6]_{0.95} \cdot 2.8H_2O$ [35] show great electrochemical performance, proving the feasibility of doping transition metals.

The introduction of carbon materials such as carbon nanotubes (CNTs) and graphene has been proved to be an effective method to improve electrode stability.[97,98] Thin films of single-walled carbon nanotubes (SWCNT) and iron-filled multi-walled carbon nanotubes (MWCNT) were prepared by Nossol *et al.* through the liquid–liquid interfacial route on plastic substrates, to obtain transparent, flexible and ITO-free electrodes.[99] The Fe species present in the two electrodes were

employed to synthesize CNT/PB nanocomposite thin films (Fig. 6a). Compared with MWCNT/PET, the SWCNT/PET electrode shows a more reversible character, while the MWCNT/PB film shows high stability after several voltammetric cycles, which is attributed to the slow diffusion of Fe species from inside of the tubes leading to a strong CNT/PB interaction. Furthermore, the research of Sun and colleagues showed that the introduction of graphene can significantly reduce the charge transfer resistance and improve the conductivity of the hybrid electrode.[100] Similarly, by combining MOF-235 ([Fe_3O $(1,4-BDC)_3(DMF)_3][FeCl_4] \cdot (DMF)_3$) with multiwall carbon nanotubes (MCNTs) and graphene, the prepared MOF-235 + 20M and MOF-235 + 20G both show better electrochemical performance (Fig. 6c and d).[101,102] The existence of interstitial water and its related decomposition lead to underestimation of the capacity of the material. With the removal of crystal water, the capacity, cycle life and coulombic efficiency of these materials will be greatly improved.[36] For example, a polypyrrole-modified PB material (KHCF@PPy) was proposed by Xue's team (Fig. 6b).[103] Through the *in situ* polymerization PPy coating method, the composite had a low defect concentration with enhanced electronic conductivity, and exhibited excellent cycling stability and rate capability. During the charge/discharge cycling test, the coulombic efficiency of the first few
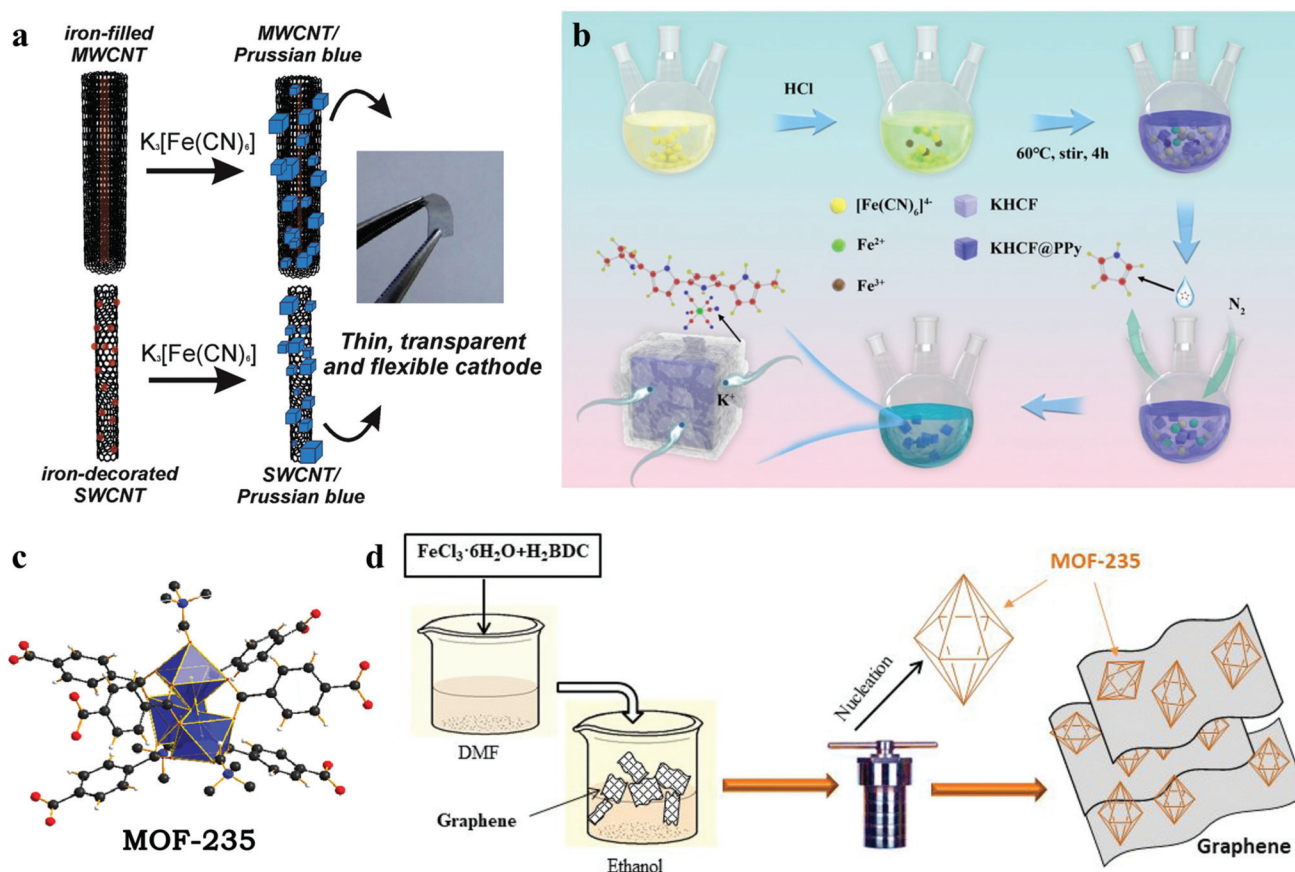

Fig. 6 (a) Schematic illustration of synthesis process of CNT/PB.[99] (b) Illustration of synthesis scheme of KHCF@PPy.[103] (c) The structural skeleton diagram of MOF-235.[101] (d) The schematic diagram of MOF-235 and graphene composites.[102]

This journal is © the Partner Organisations 2022

Inorg. Chem. Front., 2022, **9**, 827–844 | **835**

cycles is low (~72.67%), and gradually increases to above 98% of a stable level. In this process, the decomposition of residual interstitial water improves the CE.

The application of materials to full batteries is an important step towards commercialization, Zhang and colleagues elaborated on the electrochemical properties exhibited by Prussian blue as a positive material in organic electrolytes. A high performance potassium-ion battery using Prussian blue as a potassium ion cathode material also was first matched. They reported a comprehensive study on $K_{0.220}Fe[Fe(CN)_6]_{0.805} \cdot 4.01H_2O$ (KPBNPs) nanoparticles as potential cathode materials for KIBs.[104] The electrochemical reaction mechanism analysis proves that a carbon-coordinated Fe^{III}/Fe^{II} couple is the redox-active site, which is responsible for the electrochemical storage of K-ions. It is worth mentioning that this work first proposed KIB full-cell, with commercial carbon black super P as the anode and KPBNPs as the cathode. These two materials are cost-effective and essentially sustainable, showing a broad prospect of PBA in large-scale electrochemical energy storage. In the same year, another study on a KFeHCF/K_2TP full cell for non-aqueous potassium-ion batteries showed high reversible capacity of ~100 mA h g^{-1}, and better cycling performance than half cells.[105] Moreover, electrochemical measurements of the KFeHCF ($K_{1.92}Fe[Fe(CN)_6]_{0.94} \cdot 0.5H_2O$) cathode were conducted with K half-cells in several carbonate and ether mixture solutions, which indicate that the addition of fluoroethylene carbonate (FEC) effectively improves the coulombic efficiency and cycling stability.

In the applications of grid-scale stationary energy storage system, the key performance metrics are cost, cycle life, environmental compatibility, response time and energy efficiency, not energy density.[106] In order to reduce cost and improve safety, an aqueous secondary battery based on potassium shuttle ions shows great potential. It is not only much cheaper than aqueous LIBs, but also has a higher capacity than aqueous SIBs.[107–109] For example, $K_2Fe^{II}[Fe^{II}(CN)_6] \cdot 2H_2O$ nanocubes reported by Su et al. shows excellent rate performance, long cycling capability, and high reversible capacity, retaining 96% of the initial capacity even after 500 cycles at 500 mA g^{-1}.[34] Because the potassium-rich iron(II) hexacyanoferrate can provide two electrons per formula unit, the capacity is up to 120 mA h g^{-1}. In addition, by controlling the acidity of hydrothermal process, Li et al. synthesized a series of K-Prussian white nanoparticles with different sizes and gradient crystallinity.[110] In this work, they used different concentrations of hydrochloric acid aqueous solution (0, 0.2, 0.5, 1.0, 1.5, and 2.0 mol L^{-1}) to produce a gradient acidic environment, and labeled the samples as KFe(0), KFe(0.2), KFe(0.5), KFe(1.0), KFe(1.5), and KFe(2.0), respectively. The SEM images and XRD patterns show that with the increase of acidity, the particle size decreases. However, when the acidity is too high, the morphology of the particles becomes irregular with obvious agglomeration (Fig. 5e–g). Ultimately, they found that highly crystalline KFe(1.0) ($K_{1.93}Fe[Fe(CN)_6]_{0.97} \cdot 1.82H_2O$) composed of 50 nm crystallites provides the highest reversible capacity and rate capacity, and also maintained 88% of the initial capacity after 300 cycles at 1500 mA g^{-1} (Fig. 5h).

2.4. Metal–air batteries

Metal–air batteries are electrochemical reaction devices that directly convert the chemical energy of metals (magnesium, aluminium, zinc, lithium, etc.) into electrical energy, which is efficient, safe, and environmentally friendly. Although great progress has been made in the study of metal–air batteries, there are still many challenges, such as low cathode utilization and slow kinetic process at the cathode, high overpotential and poor reversibility, resulting in low actual energy density. Metal air electrodes consist of metal anodes, air cathodes, and electrolytes. Different kinds of metal–air electrodes involve different electrochemical reactions and products, depending on the metal, electrolyte, and catalytic material chosen. Table 4 summarizes the electrochemical performances of Fe-MOF based electrocatalysts for the ORR in metal–air batteries.

Zhang et al. successfully fabricated Fe-based metallopolymer nanowall composites via a simple wet-chemical process.[112] The SEM and TEM images of the Fe-based metallopolymer/reduced graphene indicated that the Fe-based metallopolymer nanowalls with 100–200 nm widths grow vertically on the graphene surface (Fig. 7d and e). The unique structure was beneficial for the improvement of catalytic activity. Through the rotating-disk setup, FMG (Fe-based metallopolymer/rGO) exhibited higher catalytic activities than CMG (Co-based metallopolymer/rGO) and MMG (Mn-based metallopolymer/rGO). The first cycle round-trip efficiencies of the FMG electrodes at current densities of 200 mA g^{-1} are 79%, but the first loop round-trip efficiencies of the CMG and MMG electrodes are 67% and 65%. Besides, hydrothermal process is also a common method for the synthesis of Fe-MOFs. Fe-BTC[113] and

Table 4 Fe-MOF based electrocatalysts for the ORR in metal–air batteries

Fe-MOF	Electrode	Supports	E_{onset}/V (vs. RHE)	$E_{1/2}$/V (vs. RHE)	Battery	Ref.
Fe-SA-NC@CC	0.1 M KOH	Carbon cloth	0.97	0.86	Al–O_2	37
ZIF-67	0.1 M KOH	$Ba_{0.5}Sr_{0.5}Co_{0.8}Fe_{0.2}O_3$	0.45	1.56	Zn–O_2	38
PCN-226	0.1 M KOH	Zr-Chains	0.83	0.75	Zn–O_2	39
FePPc@CB	0.1 M KOH	Carbon matrix	0.75	0.908	Zn–O_2	115
Ni/Fe-BTC-MOF	0.1 M KOH	—	1.091	0.964	Zn–O_2	116
HCF-MOFs	0.1 M KOH	—	0.90	0.82	Zn–O_2	117

DC: discharge capacity, CC: charge capacity, RC: reversible capacity.

836 | Inorg. Chem. Front., 2022, 9, 827–844

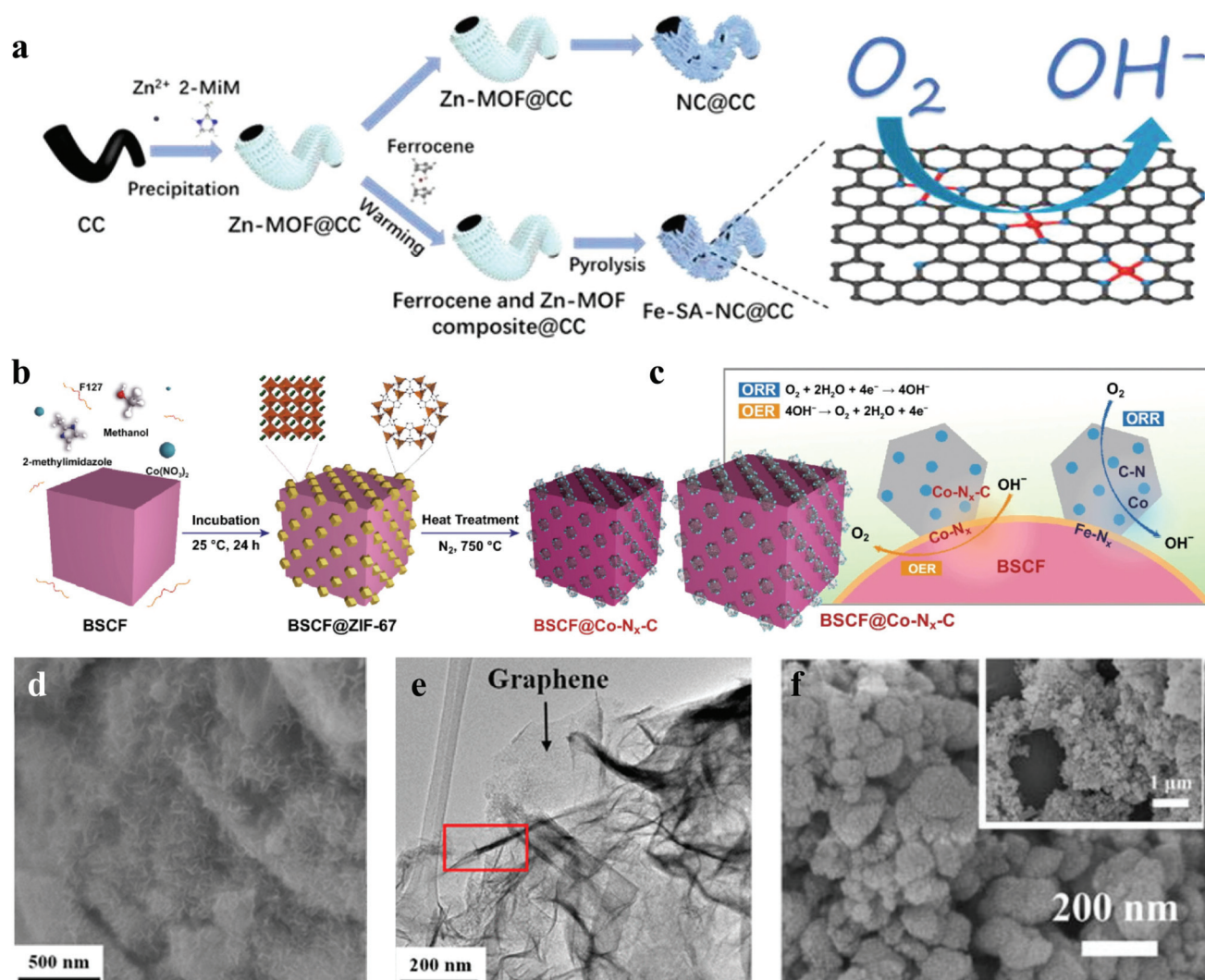This journal is © the Partner Organisations 2022

Fig. 7 (a) Schematic representation of the preparation of Fe-SA-NC@CC and NC@CC.[37] (b) Possible mechanism of the OER and ORR and for synergy between C-ZIF-67 and BSCF composites; and (c) schematic description of *in situ* growth of ZIF-67 crystals on BSCF the surface and carbonization of the prepared sample.[38] (d) SEM and (e) TEM images of Fe-based metallopolymer/reduced graphene oxide.[112] (f) SEM image of the PEF-MOF.[117]

Fe/Co-BTC[114] were prepared as excellent bifunctional catalysts through the hydrothermal process. It is noteworthy that Huang *et al.* developed a novel method utilizing gas diffusion and a subsequent pyrolysis process to synthesize Fe-SA-NC@CC (Fe-SA = iron single atoms, CC = carbon cloth) as a self-supporting electrode for the Al-air battery, which overcame the problem of inherent electrocatalytic activity and electrode configuration (Fig. 7a).[37] Owing to the coupling effect between the intrinsic ORR activity of Fe-SA and the fast ion/electron transport of nitrogen-doped carbon sheets on CC, Fe-SA-NC@CC showed enhanced ORR performance and high durability.

Fe-Based MOFs were widely used in the field of Zn-air batteries. Various approaches have been used to synthesize Fe-based MOFs. Arafat *et al.* attained BSCF@Co-Nx-C (BSFC = $Ba_{0.5}Sr0_{.5}Co_{0.8}Fe_{0.2}O_3$) by *in situ* growth of ZIF-67 obtained

from the solution of cobalt nitrate and 2-methylimidazole in the presence of BSCF particles (Fig. 7b).[38] The possible mechanism of the OER and ORR of BSCF@Co–N_x–C is shown in Fig. 7c. The N-doped porous carbon network led to effective improvement of the ORR/OER performance of the composite material. Cheng *et al.* developed a melt polymerization strategy to synthesize iron-polyphthalocyanine (FePPc) MOFs over the carbon black matrix (FePPc@CB), in which FePPc molecules could anchor on the carbon matrix, contributing to the electron transfer process and stability of the systems.[115] Additionally, Pourfarzad *et al.* applied a CES method for the fabrication of a mixed MOF, Ni/Fe-BTC, using nickel chloride and iron chloride as Ni(ɪɪ) and Fe(ɪɪ) sources, and BTC as the linker.[116] Surprisingly, zinc–air batteries with the Ni/Fe-BTC-MOF illustrated a significant cycling-life of 5262 h@10 mA cm^{-2} with an energy density of 1082 W h

This journal is © the Partner Organisations 2022

Inorg. Chem. Front., 2022, **9**, 827–844 | **837**

kg_{Zn}^{-1}. Similarly, Li *et al.* applied a bimetallic synergy strategy to attain bifunctional electrocatalysis for flexible rechargeable Zn–air batteries. The unique hierarchical structure and porous channels of HCF-MOFs ensured high exposure of metal sites (Fig. 7f), thus boosting the electrocatalytic activity.[117] Cichocka *et al.* reported a new MOF, denoted PCN-226, which was connected *via* linking redox active metalloporphyrins and Zr (+4) cations. PCN-226 was considered as a promising electrode material for rechargeable Zn–air batteries, with a high peak power density of 133 mW cm^{-2}. By using the same strategy, a series of ultra-stable porphyrinic Zr-MOFs containing metal ions such as Cu, Co, Ni, Fe and Zn were created successfully.[39]

Except metal–air batteries, Fe-based MOFs were usually applied in Li–CO$_2$ batteries. Li–CO$_2$ batteries utilize CO$_2$ gas as the reactive species, reducing the overall mass of the cell, endowing the cell with very high theoretical specific energy (up to 1876 and 1136 W h kg^{-1} for Li–CO$_2$ and Na–CO$_2$ batteries, respectively).[118,119] It has been shown that MOFs containing Fe open metal sites offer a great perspective for CO$_2$ sorption. Wongsakulphasatch *et al.* synthesized MIL-88A and MIL-127(Fe), which exhibited an excellent sorption capacity of 4.95 mmol g^{-1} for MIL-88A and 5.24 mmol g^{-1} for MIL-127 (Fe).[120] Fe(bdc) was also studied for Li–CO$_2$ batteries. However, manganese performed the best among the six metals with electrocatalytic activity studied by the authors.[121]

2.5. Lithium–sulfur batteries

Lithium–sulfur batteries, based on the electrochemical reaction of lithium and sulfur, were first proposed in the early 1960s, and have attracted extensive attention due to their theoretical specific energy of up to 2600 W h kg^{-1} and specific capacity of 1675 mA h g^{-1}, which are much higher than those of commercial lithium-ion batteries.[122] What's more, sulfur is naturally abundant, environmentally friendly and cost-effective, thus lithium–sulfur batteries have become a feasible alternative for energy storage devices in the future.[40] However, there are still several problems in the commercialization of LSBs: (1) as an insulator, sulfur leads to large electrochemical polarization and battery impedance;[123] (2) during cycling, the intermediate polysulfides may dissolve in the organic electrolyte and deposit on the lithium metal anode through the diaphragm, and operate the "shuttle effect";[124–126] and (3) the volume expansion of materials during the cycle leads to cathode failure.[127,128]

Desirable sulfur electrochemistry strongly depends on host–guest interactions, which require the rational design of the surface fine structure of sulfur reservoir materials. Zhu *et al.* first discussed the effect of coordinative unsaturation in ferric hexacyanoferrate on sulfur immobilization and catalyzation.[41] Through a simple ammonia etching treatment of FeHCF, the Fe^{III}–H$_2$O moieties were removed selectively, leaving the coordination unsaturated Fe sites with higher absorbability and conversion catalytic activity for polysulfide (Fig. 8a–e). The synthesized FeHCF-A maintained excellent rate performance and cyclability at a high current density of 5 C, including an ultra-low decay rate of 0.024% per cycle over 500 cycles and a laudable areal capacity of 4.5 mA h cm^{-2} under high sulfur loading. To develop the ideal host for sulfur, researchers turn
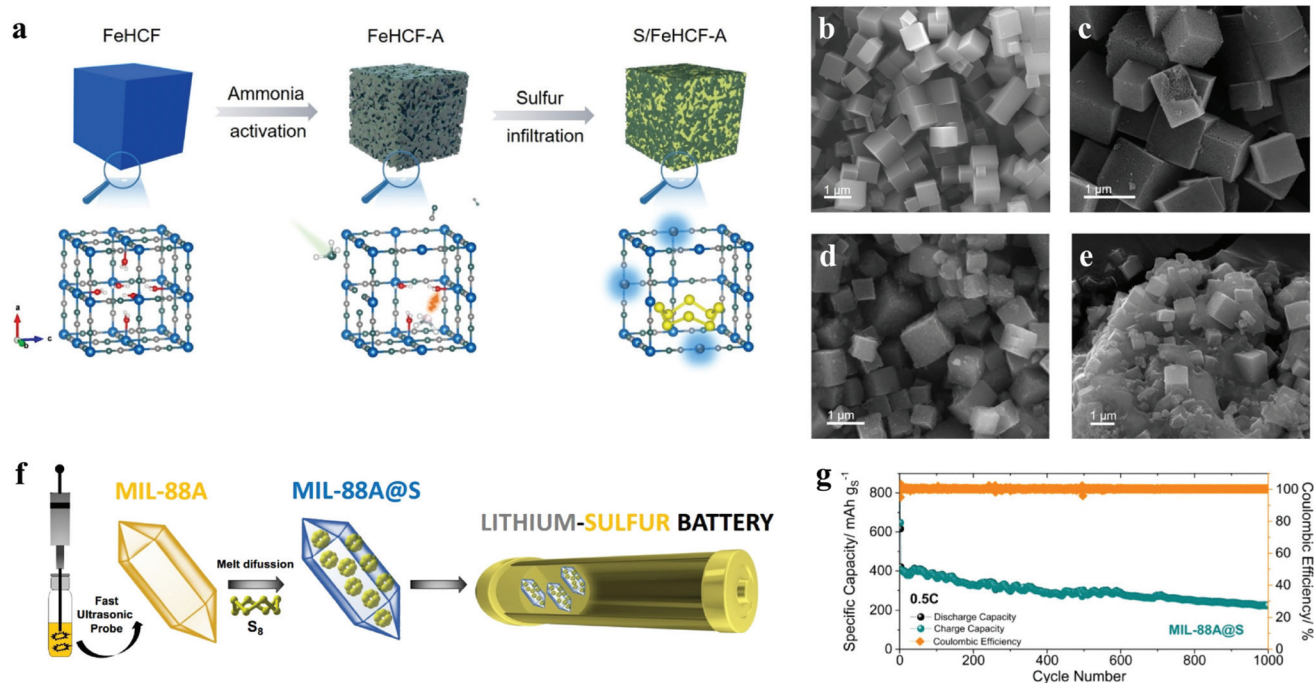

Fig. 8   (a) Schematic illustration of the synthesis of FeHCF-A and S/FeHCF-A composites; SEM image of (b) FeHCF, (c) FeHCF-A, (d) S/FeHCF-A and (e) S/FeHCF composites with sulfur (~70 wt%) loading.[41] (f) Schematic illustration of the synthesis process of MIL-88A@S; (g) long-term cycling performances tested at 0.5 C of the Li/LiTFSI-LiNO$_3$-DOL : DME/MIL-88A@S cell.[42]

their attention to MOFs with high porosity and particular morphology. Capková *et al.* prepared MIL-101(Fe)-NH$_2$, which successfully achieved sulfur capture and encapsulation.[129] As the cathode for lithium–sulfur batteries, it displayed highly stable cycle performance, high efficiency (retaining 67.6% of the initial capacity at 0.5 C after 200 cycles and the coulombic efficiency of 95%). Similarly, Benítez *et al.* synthesized MIL-88A by a sustainable, simple and short-time method with the assistance of ultrasound. The particle size (length: 900–950 nm, width: 200–250 nm) is smaller than that synthesized by a conventional solvothermal method, promoting dispersion and optimal sulfur hosting (Fig. 8f).[42] Besides, by a typical melt-diffusion method at 155 °C, the composite MIL-88A@S was prepared as the cathode material of a Li–S battery, in which sulfur was effectively confined. The MIL-88A@S electrode exhibited a stable specific capacity of 400 mA h g^{-1} at several 1 C (1 C = 1675 mA g^{-1}) and even maintained a reversible capacity of above 300 mA h g^{-1} at 0.5 C over 1000 cycles, indicative of an effective cathode material for Li–S cells with long cycles (Fig. 8g).

3. Summary and outlook

Nowadays, MOF chemistry provides more and more opportunities for the design and synthesis of battery materials due to their advantages of high specific surface area, diverse structures, simple synthesis method, controllable porous nanostructure, and excellent properties. Although Fe-MOFs are just a small branch of the MOF family, they have attracted much attention from researchers in recent years because of their abundant resources, chemical versatility, and potential practical application in life. In this review, we summarize the rapidly developing Fe-MOFs according to the classification of battery types, including synthesis methods, reaction conditions, and electrochemical properties. However, continuous efforts are needed to realize the commercial application of pristine Fe-MOF materials, and during the design process, the following issues and advise need to be considered: (1) most of the Fe-MOFs possess an appropriate porous structure and a large surface area, and a small particle size to increase the surface area, which can provide a greater contact area between the electrolyte and the active material. In addition, the nanosized structure can offer a short diffusion path for fast transport of electrons and ions to enrich electrochemical reactions. (2) Many Fe-based MOFs exhibit poor electronic conductivity and relatively low specific capacity. As a result, some conductive substrates, such as carbonaceous materials (graphene, carbon nanotubes, carbon nanofibers, *etc.*) and Cu/Ni foams, can be introduced into the framework, which has been proved to be an effective method to enhance the stability of the electrode and improve the defects of unsatisfactory energy density and poor conductivity. (3) There is search for appropriate measures to prevent the porous structure of Fe-MOFs from being mostly destroyed after calcination. Although through thermal treatment above 400 °C, the conductivity of MOFs is improved, it

will destroy the immanent organic–inorganic hybrid structure. However, by using low-temperature synthesis or other synthesis methods, different inorganic functional components can be introduced while maintaining the crystalline state and porous structure of the MOF to form "MOF–inorganic functional component" heterogeneous materials, so as to solve the problem of insufficient number of MOF active sites. Providing more active sites with metal centers or organic clusters for higher redox activity of organic linkers at high potential can achieve sufficient specific capacity; introducing electron-withdrawing groups is another method. (4) Fe-MOFs are usually prepared by the hydrothermal/solvothermal reaction between Fe salts and organic ligands, and their morphologies and compositions can be controlled by adjusting the reaction conditions including the temperature, solvent, pH, additives and molar ratio of reactants. However, due to the difficulty of accurate control of thermodynamics and kinetics in the reaction process, these two traditional and common methods sometimes lead to low yields and uneven morphologies, which is not conducive to practical application. Other feasible methods, such as dry gel conversion synthesis and microwave synthesis, are expected to be easier to operate in a short time. Therefore, further development should focus on green, large-scale synthesis techniques, through inexpensive and simple processes.

Compared with the other metallic MOFs applied in batteries, Fe-MOFs present some inherent merits and competitive advantages, such as abundant natural resources, non-toxicity, and economic benefits, together with high theoretical specific capacity and reversibility of Fe ions in redox reactions. Among different types of Fe-MOFs, the synthesis strategy of some uncommon organic ligands involve a multi-step and tedious process, making the construction of Fe-MOFs more complicated and expensive, which hinders their large-scale production and wide practical application. As a result, many literature reports mainly focus on two series of representative Fe-MOFs, namely MIL-Fe (1,4-benzenedicarboxylic acid as the ligand) and Prussian blue (ferricyanide as the ligand). Probably because these two ligands are easily commercially available and low cost, the corresponding Fe-MOFs can be fabricated with mass production and easy modifications. In particular, as for Prussian blue and Prussian blue analogues, controllable morphology can be achieved in many cases through simple synthesis routes and at mild reaction temperatures. Although tremendous efforts have been devoted to design and develop new Fe-MOF structures with versatile redox activity as advanced electrode materials, more accurate control of the chemical composition and fine nanostructures still faces challenges. Additionally, in place of using a single metal to grow Fe-MOFs, a multimetallic source can be used to prepare heterometallic Fe-based MOFs, which will be a promising application to enhance the electrochemical properties owing to the synergistic effect. Systematic experimental research and predictive theoretical modeling are important to better clarify and understand the relationship between Fe-MOF nanostructures and their properties in various energy applications. Overall, we hope to provide researchers with relevant experience in syn-

This journal is © the Partner Organisations 2022

Inorg. Chem. Front., 2022, **9**, 827–844 | **839**

thesis processes and improved methods for Fe-MOFs through this review, and attract more attention to explore this fascinating field.

Conflicts of interest

There are no conflicts to declare.

Acknowledgements

Notes and references

1 J. Montero, D. Arenas-Esteban, D. Ávila-Brande, E. Castillo-Martínez, S. Licoccia and J. Carretero-González, Lithium ion storage in 1d and 2d redox active metal-organic frameworks, *Electrochim. Acta*, 2020, **341**, 136063.

2 Q. Zhang, E. Uchaker, S. L. Candelaria and G. Cao, Nanomaterials for energy conversion and storage, *Chem. Soc. Rev.*, 2013, **42**, 3127–3171.

3 M. M. Thackeray, C. Wolverton and E. D. Isaacs, Electrical energy storage for transportation-approaching the limits of, and going beyond, lithium-ion batteries, *Energy Environ. Sci.*, 2012, **5**, 7854–7863.

4 S. Chu, Y. Cui and N. Liu, The path towards sustainable energy, *Nat. Mater.*, 2016, **16**, 16–22.

5 P. Leung, A. A. Shah, L. Sanz, C. Flox, J. R. Morante, Q. Xu, M. R. Mohamed, C. Ponce de León and F. C. Walsh, Recent developments in organic redox flow batteries: A critical review, *J. Power Sources*, 2017, **360**, 243–283.

6 L. Shen, H. Song and C. Wang, Metal-organic frameworks triggered high-efficiency li storage in Fe-based polyhedral nanorods for lithium-ion batteries, *Electrochim. Acta*, 2017, **235**, 595–603.

7 Y. Lee, J. Kim and W. Ahn, Synthesis of metal-organic frameworks: A mini review, *Korean J. Chem. Eng.*, 2013, **30**, 1667–1680.

8 C. Li, X. Lou, M. Shen, X. Hu, Z. Guo, Y. Wang, B. Hu and Q. Chen, High anodic performance of Co 1,3,5-benzenetricarboxylate coordination polymers for Li-ion battery, *ACS Appl. Mater. Interfaces*, 2016, **8**, 15352–15360.

9 S. Maiti, A. Pramanik, U. Manju and S. Mahanty, $Cu_3(1,3,5\text{-benzenetricarboxylate})_2$ metal-organic framework: A promising anode material for lithium-ion battery, *Microporous Mesoporous Mater.*, 2016, **226**, 353–359.

10 Y. Liang, Z. Tao and J. Chen, Organic electrode materials for rechargeable lithium batteries, *Adv. Energy Mater.*, 2012, **2**, 742–769.

11 A. Morozan and F. Jaouen, Metal organic frameworks for electrochemical applications, *Energy Environ. Sci.*, 2012, **5**, 9269–9290.

12 B. Liu, H. Shioyama, H. Jiang, X. Zhang and Q. Xu, Metal–organic framework (MOF) as a template for syntheses of nanoporous carbons as electrode materials for supercapacitor, *Carbon*, 2010, **48**, 456–463.

13 Q. L. Zhu and Q. Xu, Metal-organic framework composites, *Chem. Soc. Rev.*, 2014, **43**, 5468–5512.

14 J. R. Li, R. J. Kuppler and H. C. Zhou, Selective gas adsorption and separation in metal-organic frameworks, *Chem. Soc. Rev.*, 2009, **38**, 1477–1504.

15 T. R. Whitfield, X. Wang, L. Liu and A. J. Jacobson, Metal-organic frameworks based on iron oxide octahedral chains connected by benzenedicarboxylate dianions, *Solid State Sci.*, 2005, **7**, 1096–1103.

16 E. D. Bloch, L. J. Murray, W. L. Queen, S. Chavan, S. N. Maximoff, J. P. Bigi, R. Krishna, V. K. Peterson, F. Grandjean, G. J. Long, B. Smit, S. Bordiga, C. M. Brown and J. R. Long, Selective binding of O_2 over N_2 in a redox-active metal-organic framework with open iron(II) coordination sites, *J. Am. Chem. Soc.*, 2011, **133**, 14814–14822.

17 A. Dhakshinamoorthy, M. Alvaro and H. Garcia, Aerobic oxidation of benzylic alcohols catalyzed by metal–organic frameworks assisted by tempo, *ACS Catal.*, 2010, **1**, 48–53.

18 M. Yang, Y. Zhou, Y. Cao, Z. Tong, B. Dong and Y. Chai, Advances and challenges of Fe-MOFs based materials as electrocatalysts for water splitting, *Appl. Mater. Today*, 2020, **20**, 100692.

19 J. S. Lee, S. H. Jhung, J. W. Yoon, Y. K. Hwang and J. S. Chang, Adsorption of methane on porous metal carboxylates, *J. Ind. Eng. Chem.*, 2009, **15**, 674–676.

20 S. Duan, J. Li, X. Liu, Y. Wang, S. Zeng, D. Shao and T. Hayat, HF-free synthesis of nanoscale metal–organic framework NMIL-100(Fe) as an efficient dye adsorbent, *ACS Sustainable Chem. Eng.*, 2016, **4**, 3368–3378.

21 A. Dhakshinamoorthy, M. Alvaro, H. Chevreau, P. Horcajada, T. Devic, C. Serre and H. Garcia, Iron(III) metal–organic frameworks as solid lewis acids for the isomerization of α-pinene oxide, *Catal. Sci. Technol.*, 2012, **2**, 324–330.

22 Q. Xia, H. Wang, B. Huang, X. Yuan, J. Zhang, J. Zhang, L. Jiang, T. Xiong and G. Zeng, State-of-the-art advances and challenges of iron-based metal organic frameworks from attractive features, synthesis to multifunctional applications, *Small*, 2019, **15**, 1803088.

23 G. Férey, F. Millange, M. Morcrette, C. Serre, M. L. Doublet, J. M. Greneche and J. M. Tarascon, Mixed-valence Li/Fe-based metal-organic frameworks with both reversible redox and sorption properties, *Angew. Chem., Int. Ed.*, 2007, **46**, 3259–3263.

24 A. Fateeva, P. Horcajada, T. Devic, C. Serre, J. Marrot, J.-M. Grenèche, M. Morcrette, J.-M. Tarascon, G. Maurin

840 | *Inorg. Chem. Front.*, 2022, **9**, 827–844

This journal is © the Partner Organisations 2022

and G. Férey, Synthesis, structure, characterization, and redox properties of the porous MIL-68(Fe) solid, *Eur. J. Inorg. Chem.*, 2010, **24**, 3789–3794.

25 Y. Jin, C. Zhao, Y. Lin, D. Wang, L. Chen and C. Shen, Fe-based metal-organic framework and its derivatives for reversible lithium storage, *J. Mater. Sci. Technol.*, 2017, **33**, 768–774.

26 J. Shin, M. Kim, J. Cirera, S. Chen, G. J. Halder, T. A. Yersak, F. Paesani, S. M. Cohen and Y. S. Meng, MIL-101(Fe) as a lithium-ion battery electrode material: A relaxation and intercalation mechanism during lithium insertion, *J. Mater. Chem. A*, 2015, **3**, 4738–4744.

27 M. E. Ziebel, C. A. Gaggioli, A. B. Turkiewicz, W. Ryu, L. Gagliardi and J. R. Long, Effects of covalency on anionic redox chemistry in semiquinoid-based metal-organic frameworks, *J. Am. Chem. Soc.*, 2020, **142**, 2653–2664.

28 D. Zhou, J. Ni and L. Li, Self-supported multicomponent CPO-27 MOF nanoarrays as high-performance anode for lithium storage, *Nano Energy*, 2019, **57**, 711–717.

29 X. Zhao, G. Niu, H. Yang, J. Ma, M. Sun, M. Xu, W. Xiong, T. Yang, L. Chen and C. Wang, MIL-88A@polyoxometalate microrods as an advanced anode for high-performance lithium ion batteries, *CrystEngComm*, 2020, **22**, 3588–3597.

30 X. Wang, R. Kurono, S. Nishimura, M. Okubo and A. Yamada, Iron-oxalato framework with one-dimensional open channels for electrochemical sodium-ion intercalation, *Chem. – Eur. J.*, 2015, **21**, 1096–1101.

31 P. Nie, L. Shen, G. Pang, Y. Zhu, G. Xu, Y. Qing, H. Dou and X. Zhang, Flexible metal–organic frameworks as superior cathodes for rechargeable sodium-ion batteries, *J. Mater. Chem. A*, 2015, **3**, 16590–16597.

32 W. Zhang, Y. Zhao, V. Malgras, Q. Ji, D. Jiang, R. Qi, K. Ariga, Y. Yamauchi, J. Liu, J. S. Jiang and M. Hu, Synthesis of monocrystalline nanoframes of prussian blue analogues by controlled preferential etching, *Angew. Chem., Int. Ed.*, 2016, **55**, 8228–8234.

33 J. W. Heo, M. S. Chae, J. Hyoung and S. T. Hong, Rhombohedral potassium-zinc hexacyanoferrate as a cathode material for nonaqueous potassium-ion batteries, *Inorg. Chem.*, 2019, **58**, 3065–3072.

34 D. Su, A. McDonagh, S. Z. Qiao and G. Wang, High-capacity aqueous potassium-ion batteries for large-scale energy storage, *Adv. Mater.*, 2017, **29**, 1604007.

35 Y. Luo, B. Shen, B. Guo, L. Hu, Q. Xu, R. Zhan, Y. Zhang, S. Bao and M. Xu, Potassium titanium hexacyanoferrate as a cathode material for potassium-ion batteries, *J. Phys. Chem. Solids*, 2018, **122**, 31–35.

36 X. Wu, Z. Jian, Z. Li and X. Ji, Prussian white analogues as promising cathode for non-aqueous potassium-ion batteries, *Electrochem. Commun.*, 2017, **77**, 54–57.

37 L. Huang, W. Zang, Y. Ma, C. Zhu, D. Cai, H. Chen, J. Zhang, H. Yu, Q. Zou, L. Wu and C. Guan, In-situ formation of isolated iron sites coordinated on nitrogen-doped carbon coated carbon cloth as self-supporting elec-trode for flexible aluminum-air battery, *Chem. Eng. J.*, 2021, **421**, 129973.

38 Y. Arafat, M. R. Azhar, Y. Zhong, X. Xu, M. O. Tadé and Z. Shao, A porous nano-micro-composite as a high-performance bi-functional air electrode with remarkable stability for rechargeable zinc–air batteries, *Nano-Micro Lett.*, 2020, **12**, 130.

39 M. O. Cichocka, Z. Liang, D. Feng, S. Back, S. Siahrostami, X. Wang, L. Samperisi, Y. Sun, H. Xu, N. Hedin, H. Zheng, X. Zou, H. C. Zhou and Z. Huang, A porphyrinic zirconium metal-organic framework for oxygen reduction reaction: Tailoring the spacing between active-sites through chain-based inorganic building units, *J. Am. Chem. Soc.*, 2020, **142**, 15386–15395.

40 L. Zhou, D. L. Danilov, R. A. Eichel and P. H. L. Notten, Host materials anchoring polysulfides in Li–S batteries reviewed, *Adv. Energy Mater.*, 2020, **11**, 2001304.

41 Y. Zhu, G. Li, D. Luo, H. Wan, M. Feng, D. Yuan, W. Hu, Z. Li, R. Gao, Z. Zhang, W. Liu, M. Li, Y. Deng, L. Wang, Y. Hu, X. Chen and Z. Chen, Unsaturated coordination polymer frameworks as multifunctional sulfur reservoir for fast and durable lithium-sulfur batteries, *Nano Energy*, 2021, **79**, 105393.

42 A. Benitez, J. Amaro-Gahete, D. Esquivel, F. J. Romero-Salguero, J. Morales and A. Caballero, MIL-88A metal-organic framework as a stable sulfur-host cathode for long-cycle Li-S batteries, *Nanomaterials*, 2020, **10**, 424.

43 J. B. Goodenough, Electrochemical energy storage in a sustainable modern society, *Energy Environ. Sci.*, 2014, **7**, 14–18.

44 M. Armand and J. M. Tarascon, Building better batteries, *Nature*, 2008, **451**, 652–657.

45 J. M. Tarascon, Towards sustainable and renewable systems for electrochemical energy storage, *ChemSusChem*, 2008, **1**, 777–779.

46 G. de Combarieu, M. Morcrette, F. Millange, N. Guillou, J. Cabana, C. P. Grey, I. Margiolaki, G. Férey and J. M. Tarascon, Influence of the benzoquinone sorption on the structure and electrochemical performance of the MIL-53(Fe) hybrid porous material in a lithium-ion battery, *Chem. Mater.*, 2009, **21**, 1602–1611.

47 C. Li, C. Zhang, J. Xie, K. Wang, J. Li and Q. Zhang, Ferrocene-based metal-organic framework as a promising cathode in lithium-ion battery, *Chem. Eng. J.*, 2021, **404**, 126463.

48 C. Zhang, W. Hu, H. Jiang, J. K. Chang, M. Zheng, Q. H. Wu and Q. Dong, Electrochemical performance of MIL-53(Fe)@RGO as an organic anode material for li-ion batteries, *Electrochim. Acta*, 2017, **246**, 528–535.

49 S. Zheng, X. Li, B. Yan, Q. Hu, Y. Xu, X. Xiao, H. Xue and H. Pang, Transition-metal (Fe, Co, Ni) based metal-organic frameworks for electrochemical energy storage, *Adv. Energy Mater.*, 2017, **7**, 1602733.

50 J. Ni, Y. Zhao, L. Li and L. Mai, Ultrathin MoO_2 nanosheets for superior lithium storage, *Nano Energy*, 2015, **11**, 129–135.

This journal is © the Partner Organisations 2022

Inorg. Chem. Front., 2022, **9**, 827–844 | **841**

51 R. R. Salunkhe, Y. V. Kaneti, J. Kim, J. H. Kim and Y. Yamauchi, Nanoarchitectures for metal-organic framework-derived nanoporous carbons toward supercapacitor applications, *Acc. Chem. Res.*, 2016, **49**, 2796–2806.

52 Z. Liang, C. Qu, W. Guo, R. Zou and Q. Xu, Pristine metal-organic frameworks and their composites for energy storage and conversion, *Adv. Mater.*, 2018, **30**, 1702891.

53 L. Sun, J. Xie, Z. Chen, J. Wu and L. Li, Reversible lithium storage in a porphyrin-based MOF (PCN-600) with exceptionally high capacity and stability, *Dalton Trans.*, 2018, **47**, 9989–9993.

54 L. Cosimbescu, X. Wei, M. Vijayakumar, W. Xu, M. L. Helm, S. D. Burton, C. M. Sorensen, J. Liu, V. Sprenkle and W. Wang, Anion-tunable properties and electrochemical performance of functionalized ferrocene compounds, *Sci. Rep.*, 2015, **5**, 14117.

55 C. Li, H. Yang, J. Xie, K. Wang, J. Li and Q. Zhang, Ferrocene-based mixed-valence metal-organic framework as an efficient and stable cathode for lithium-ion-based dual-ion battery, *ACS Appl. Mater. Interfaces*, 2020, **12**, 32719–32725.

56 S. M. Batterjee, M. I. Marzouk, M. E. Aazab and M. A. El-Hashash, The electrochemistry of some ferrocene derivatives: Redox potential and substituent effects, *Appl. Organomet. Chem.*, 2003, **17**, 291–297.

57 J. Xie and Q. Zhang, Recent progress in multivalent metal (Mg, Zn, Ca, and Al) and metal-ion rechargeable batteries with organic materials as promising electrodes, *Small*, 2019, **15**, 1805061.

58 J. Hu, H. Diao, W. Luo and Y. F. Song, Dawson-type polyoxomolybdate anions $(P_2Mo_{18}O_{62}^{6-})$ captured by ionic liquid on graphene oxide as high-capacity anode material for lithium-ion batteries, *Chem. – Eur. J.*, 2017, **23**, 8729–8735.

59 J. Xie, Y. Zhang, Y. Han and C. Li, High-capacity molecular scale conversion anode enabled by hybridizing cluster-type framework of high loading with amino-functionalized graphene, *ACS Nano*, 2016, **10**, 5304–5313.

60 Z. Wang, L. M. Zheng, M. Jagodic, Z. Jaglicic, H. F. Su, J. X. Zhuang, X. P. Wang, C. H. Tung and D. Sun, A polyoxochromate templated 56-nuclei silver nanocluster, *Inorg. Chem.*, 2020, **59**, 3004–3011.

61 J. J. Chen, M. D. Symes, S. C. Fan, M. S. Zheng, H. N. Miras, Q. F. Dong and L. Cronin, High-performance polyoxometalate-based cathode materials for rechargeable lithium-ion batteries, *Adv. Mater.*, 2015, **27**, 4649–4654.

62 M. Zhang, A. M. Zhang, X. X. Wang, Q. Huang, X. Zhu, X. L. Wang, L. Z. Dong, S. L. Li and Y. Q. Lan, Encapsulating ionic liquids into POM-based MOFs to improve their conductivity for superior lithium storage, *J. Mater. Chem. A*, 2018, **6**, 8735–8741.

63 Y. Ai, Z. Han, X. Jiang, H. Luo, J. Cui, Q. Bao, C. Jing, J. Fu, J. Cheng and S. Liu, General construction of 2d ordered mesoporous iron-based metal-organic nanomeshes, *Small*, 2020, **16**, 2002701.

64 T. Yamada, K. Shiraishi and N. Kimizuka, Synthesis of a redox-active metal–organic framework MIL-116(Fe) and its lithium ion battery cathode properties, *Chem. Lett.*, 2019, **48**, 1379–1382.

65 K. Zhang, R. S. Varma, H. W. Jang, J.-W. Choi and M. Shokouhimehr, +iron hexacyanocobaltate metal-organic framework: Highly reversible and stationary electrode material with rich borders for lithium-ion batteries, *J. Alloys Compd.*, 2019, **791**, 911–917.

66 X. Hu, X. Lou, C. Li, Y. Ning, Y. Liao, Q. Chen, E. S. Mananga, M. Shen and B. Hu, Facile synthesis of the basolite F300-like nanoscale Fe-BTC framework and its lithium storage properties, *RSC Adv.*, 2016, **6**, 114483–114490.

67 N. Sharma, S. Szunerits, R. Boukherroub, R. Ye, S. Melinte, M. O. Thotiyl and S. Ogale, Dual-ligand Fe-metal organic framework based robust high capacity Li ion battery anode and its use in a flexible battery format for electro-thermal heating, *ACS Appl. Energy Mater.*, 2019, **2**, 4450–4457.

68 Y. Nishi, Lithium ion secondary batteries; past 10 years and the future, *J. Power Sources*, 2001, **100**, 101–106.

69 N. Yabuuchi, K. Kubota, M. Dahbi and S. Komaba, Research development on sodium-ion batteries, *Chem. Rev.*, 2014, **114**, 11636–11682.

70 J. Y. Hwang, S. T. Myung and Y. K. Sun, Sodium-ion batteries: Present and future, *Chem. Soc. Rev.*, 2017, **46**, 3529–3614.

71 H. Pan, Y. Hu and L. Chen, Room-temperature stationary sodium-ion batteries for large-scale electric energy storage, *Energy Environ. Sci.*, 2013, **6**, 2338–2360.

72 D. Kundu, E. Talaie, V. Duffort and L. F. Nazar, The emerging chemistry of sodium ion batteries for electrochemical energy storage, *Angew. Chem., Int. Ed.*, 2015, **54**, 3431–3448.

73 J. S. Chavez, K. L. Harrison and D. F. Sava Gallis, Na intercalation in Fe-MIL-100 for aqueous Na-ion batteries, *RSC Adv.*, 2017, **7**, 24312–24320.

74 M. B. Hursthouse, M. E. Light and D. J. Price, One-dimensional magnetism in anhydrous iron and cobalt ternary oxalates with rare trigonal-prismatic metal coordination environment, *Angew. Chem., Int. Ed.*, 2004, **43**, 472–475.

75 C. Train, M. Gruselle and M. Verdaguer, The fruitful introduction of chirality and control of absolute configurations in molecular magnets, *Chem. Soc. Rev.*, 2011, **40**, 3297–3312.

76 Y. Yue, P. F. Fulvio and S. Dai, Hierarchical metal-organic framework hybrids: Perturbation-assisted nanofusion synthesis, *Acc. Chem. Res.*, 2015, **48**, 3044–3052.

77 Q. Yang, W. Wang, H. Li, J. Zhang, F. Kang and B. Li, Investigation of iron hexacyanoferrate as a high rate cathode for aqueous batteries: Sodium-ion batteries and lithium-ion batteries, *Electrochim. Acta*, 2018, **270**, 96–103.

78 C. Tan, X. Cao, X. J. Wu, Q. He, J. Yang, X. Zhang, J. Chen, W. Zhao, S. Han, G. H. Nam, M. Sindoro and H. Zhang,

842 | *Inorg. Chem. Front.*, 2022, **9**, 827–844

This journal is © the Partner Organisations 2022

Recent advances in ultrathin two-dimensional nano-materials, *Chem. Rev.*, 2017, **117**, 6225–6331.

79 T. Wang, S. Chen, H. Pang, H. Xue and Y. Yu, MoS_2-based nanocomposites for electrochemical energy storage, *Adv. Sci.*, 2017, **4**, 1600289.

80 M. Morant-Giner, R. Sanchis-Gual, J. Romero, A. Alberola, L. García-Cruz, S. Agouram, M. Galbiati, N. M. Padial, J. C. Waerenborgh, C. Martí-Gastaldo, S. Tatay, A. Forment-Aliaga and E. Coronado, Prussian blue@MoS_2 layer composites as highly efficient cathodes for sodium- and potassium-ion batteries, *Adv. Funct. Mater.*, 2018, **28**, 1706125.

81 M. A. Mahmoud, W. Qian and M. A. El-Sayed, Following charge separation on the nanoscale in Cu_2O-Au nano-frame hollow nanoparticles, *Nano Lett.*, 2011, **11**, 3285–3289.

82 C. Chen, Y. Kang, Z. Huo, Z. Zhu, W. Huang, H. L. Xin, J. D. Snyder, D. Li, J. A. Herron, M. Mavrikakis, M. Chi, K. L. More, Y. Li, N. M. Markovic, G. A. Somorjai, P. Yang and V. R. Stamenkovic, Highly crystalline multimetallic nanoframes with three-dimensional electrocatalytic surfaces, *Science*, 2014, **343**, 1339–1343.

83 Y. Marcus, Thermodynamic functions of transfer of single ions from water to nonaqueous and mixed solvents: Part 3 - standard potentials of selected electrodes, *Pure Appl. Chem.*, 1985, **57**, 1129–1132.

84 C. Vaalma, G. A. Giffin, D. Buchholz and S. Passerini, Non-aqueous K-ion battery based on layered $K_{0.3}MnO_2$ and hard carbon/carbon black, *J. Electrochem. Soc.*, 2016, **163**, 1295–1299.

85 J. Han, G. N. Li, F. Liu, M. Wang, Y. Zhang, L. Hu, C. Dai and M. Xu, Investigation of $K_3V_2(PO_4)_3$/C nanocomposites as high-potential cathode materials for potassium-ion batteries, *Chem. Commun.*, 2017, **53**, 1805–1808.

86 L. Wang, Y. Lu, J. Liu, M. Xu, J. Cheng, D. Zhang and J. B. Goodenough, A superior low-cost cathode for a Na-ion battery, *Angew. Chem., Int. Ed.*, 2013, **52**, 1964–1967.

87 P. Padigi, J. Thiebes, M. Swan, G. Goncher, D. Evans and R. Solanki, Prussian green: A high rate capacity cathode for potassium ion batteries, *Electrochim. Acta*, 2015, **166**, 32–39.

88 N. Imanishi, T. Morikawa, J. Kondo, Y. Takeda, O. Yamamoto, N. Kinugasa and T. Yamagishi, Lithium intercalation behavior into iron cyanide complex as positive electrode of lithium secondary battery, *J. Power Sources*, 1999, **79**, 215–219.

89 N. Imanishi, T. Morikawa, J. Kondo, R. Yamane, Y. Takeda, O. Yamamoto, H. Sakaebe and M. Tabuchi, Lithium intercalation behavior of iron cyanometallates, *J. Power Sources*, 1999, **81**, 530–534.

90 K. Itaya, T. Ataka and S. Toshima, Spectroelectrochemistry and electrochemical preparation method of prussian blue modified electrodes, *J. Am. Chem. Soc.*, 2002, **104**, 4767–4772.

91 A. Eftekhari, Potassium secondary cell based on prussian blue cathode, *J. Power Sources*, 2004, **126**, 221–228.

92 M. Qin, W. Ren, J. Meng, X. Wang, X. Yao, Y. Ke, Q. Li and L. Mai, Realizing superior prussian blue positive electrode for potassium storage via ultrathin nanosheet assembly, *ACS Sustainable Chem. Eng.*, 2019, **7**, 11564–11570.

93 S. Chong, Y. Chen, Y. Zheng, Q. Tan, C. Shu, Y. Liu and Z. Guo, Potassium ferrous ferricyanide nanoparticles as a high capacity and ultralong life cathode material for non-aqueous potassium-ion batteries, *J. Mater. Chem. A*, 2017, **5**, 22465–22471.

94 B. Huang, Y. Shao, Y. Liu, Z. Lu, X. Lu and S. Liao, Improving potassium-ion batteries by optimizing the composition of prussian blue cathode, *ACS Appl. Energy Mater.*, 2019, **2**, 6528–6535.

95 B. Huang, Y. Liu, Z. Lu, M. Shen, J. Zhou, J. Ren, X. Li and S. Liao, Prussian blue $[K_2FeFe(CN)_6]$ doped with nickel as a superior cathode: An efficient strategy to enhance potassium storage performance, *ACS Sustainable Chem. Eng.*, 2019, **7**, 16659–16667.

96 X. Bie, K. Kubota, T. Hosaka, K. Chihara and S. Komaba, A novel K-ion battery: Hexacyanoferrate(ii)/graphite cell, *J. Mater. Chem. A*, 2017, **5**, 4325–4330.

97 A. Fagan-Murphy, M. C. Allen and B. A. Patel, Chemically modified multiwall carbon nanotube composite electrodes: An assessment of fabrication strategies, *Electrochim. Acta*, 2015, **152**, 249–254.

98 Z. Li, J. Chen, W. Li, K. Chen, L. Nie and S. Yao, Improved electrochemical properties of prussian blue by multi-walled carbon nanotubes, *J. Electroanal. Chem.*, 2007, **603**, 59–66.

99 E. Nossol, V. H. Souza and A. J. Zarbin, Carbon nanotube/prussian blue thin films as cathodes for flexible, transparent and ITO-free potassium secondary battery, *J. Colloid Interface Sci.*, 2016, **478**, 107–116.

100 Y. Sun, C. Liu, J. Xie, D. Zhuang, W. Zheng and X. Zhao, Potassium manganese hexacyanoferrate/graphene as a high-performance cathode for potassium-ion batteries, *New J. Chem.*, 2019, **43**, 11618–11625.

101 Q. Deng, S. Feng, P. Hui, H. Chen, C. Tian, R. Yang and Y. Xu, Exploration of low-cost microporous Fe(III)-based organic framework as anode material for potassium-ion batteries, *J. Alloys Compd.*, 2020, **830**, 154714.

102 Q. Deng, Z. Luo, H. Liu, Y. Zhou, C. Zhou, R. Yang, L. Wang, Y. Yan and Y. Xu, Facile synthesis of Fe-based metal-organic framework and graphene composite as an anode material for K-ion batteries, *Ionics*, 2020, **26**, 5565–5573.

103 Q. Xue, L. Li, Y. Huang, R. Huang, F. Wu and R. Chen, Polypyrrole-modified prussian blue cathode material for potassium ion batteries via in situ polymerization coating, *ACS Appl. Mater. Interfaces*, 2019, **11**, 22339–22345.

104 C. Zhang, Y. Xu, M. Zhou, L. Liang, H. Dong, M. Wu, Y. Yang and Y. Lei, Potassium prussian blue nano-particles: A low-cost cathode material for potassium-ion batteries, *Adv. Funct. Mater.*, 2017, **27**, 1604307.

105 J. Liao, Q. Hu, Y. Yu, H. Wang, Z. Tang, Z. Wen and C. Chen, Potassium-rich iron hexacyanoferrate/dipotas-

sium terephthalate@carbon nanotube composite used for K-ion full-cells with an optimized electrolyte, *J. Mater. Chem. A*, 2017, **5**, 19017–19024.

106 H. W. Lee, M. Pasta, R. Y. Wang, R. Ruffo and Y. Cui, Effect of the alkali insertion ion on the electrochemical properties of nickel hexacyanoferrate electrodes, *Faraday Discuss.*, 2014, **176**, 69–81.

107 J. Y. Luo and Y. Y. Xia, Aqueous lithium-ion battery LiTi$_2$(PO$_4$)$_3$/LiMn$_2$O$_4$ with high power and energy densities as well as superior cycling stability, *Adv. Funct. Mater.*, 2007, **17**, 3877–3884.

108 J. Y. Luo, W. J. Cui, P. He and Y. Y. Xia, Raising the cycling stability of aqueous lithium-ion batteries by eliminating oxygen in the electrolyte, *Nat. Chem.*, 2010, **2**, 760–765.

109 Z. Li, D. Young, K. Xiang, W. C. Carter and Y. M. Chiang, Towards high power high energy aqueous sodium-ion batteries: The NaTi$_2$(PO$_4$)$_3$/Na$_{0.44}$MnO$_2$ system, *Adv. Energy Mater.*, 2013, **3**, 290–294.

110 C. Li, X. Wang, W. Deng, C. Liu, J. Chen, R. Li and M. Xue, Size engineering and crystallinity control enable high–capacity aqueous potassium–ion storage of prussian white analogues, *ChemElectroChem*, 2018, **5**, 3887–3892.

111 G. He and L. F. Nazar, Crystallite size control of prussian white analogues for nonaqueous potassium-ion batteries, *ACS Energy Lett.*, 2017, **2**, 1122–1127.

112 W. Zhang, J. Zhu, H. Ang, H. Wang, H. T. Tan, D. Yang, C. Xu, N. Xiao, B. Li, W. Liu, X. Wang, H. H. Hng and Q. Yan, Fe-based metallopolymer nanowall-based composites for Li-O$_2$ battery cathode, *ACS Appl. Mater. Interfaces*, 2014, **6**, 7164–7170.

113 G. Song, Z. Wang, L. Wang, G. Li, M. Huang and F. Yin, Preparation of MOF(Fe) and its catalytic activity for oxygen reduction reaction in an alkaline electrolyte, *Chin. J. Catal.*, 2014, **35**, 185–195.

114 H. Wang, F. Yin, G. Li, B. Chen and Z. Wang, Preparation, characterization and bifunctional catalytic properties of MOF(Fe/Co) catalyst for oxygen reduction/evolution reactions in alkaline electrolyte, *Int. J. Hydrogen Energy*, 2014, **39**, 16179–16186.

115 W. Z. Cheng, J. L. Liang, H. B. Yin, Y. J. Wang, W. F. Yan and J. N. Zhang, Bifunctional iron-phtalocyanine metal–organic framework catalyst for ORR, OER and rechargeable zinc–air battery, *Rare Met.*, 2020, **39**, 815–823.

116 H. Pourfarzad, M. Shabani-Nooshabadi and M. R. Ganjali, Novel bi-functional electrocatalysts based on the electrochemical synthesized bimetallicmetal organic frameworks: Towards high energy advanced reversible zinc–air batteries, *J. Power Sources*, 2020, **451**, 227768.

117 W. Li, C. Wu, H. Ren, W. Fang, L. Zhao and K. N. Dinh, Hybrid cobalt and iron based metal organic framework composites as efficient bifunctional electrocatalysts towards long-lasting flexible zinc-air batteries, *Batteries Supercaps*, 2020, **3**, 1321–1328.

118 A. Khurram, M. He and B. M. Gallant, Tailoring the discharge reaction in Li-CO$_2$ batteries through incorporation of CO$_2$ capture chemistry, *Joule*, 2018, **2**, 2649–2666.

119 F. Cai, Z. Hu and S. L. Chou, Progress and future perspectives on Li(Na)-CO$_2$ batteries, *Adv. Sustainable Syst.*, 2018, **2**, 1800060.

120 S. Wongsakulphasatch, W. Kiatkittipong, J. Saupsor, J. Chaiwiseshphol, P. Piroonlerkgul, V. Parasuk and S. Assabumrungrat, Effect of Fe open metal site in metal-organic frameworks on post-combustion CO$_2$ capture performance, *Greenhouse Gases: Sci. Technol.*, 2017, **7**, 383–394.

121 S. Li, Y. Dong, J. Zhou, Y. Liu, J. Wang, X. Gao, Y. Han, P. Qi and B. Wang, Carbon dioxide in the cage: Manganese metal–organic frameworks for high performance CO$_2$ electrodes in Li–CO$_2$ batteries, *Energy Environ. Sci.*, 2018, **11**, 1318–1325.

122 L. Zhou, D. L. Danilov, R.-A. Eichel and P. H. L. Notten, Host materials anchoring polysulfides in Li-S batteries reviewed, *Adv. Energy Mater.*, 2021, **11**, 2001304.

123 D. Capková, T. Kazda, A. S. Fedorková, P. Čudek and R. Oriňaková, Carbon materials as the matrices for sulfur in Li-S batteries, *ECS Trans.*, 2019, **95**, 19–26.

124 N. Jayaprakash, J. Shen, S. S. Moganty, A. Corona and L. A. Archer, Porous hollow carbon@sulfur composites for high-power lithium-sulfur batteries, *Angew. Chem., Int. Ed.*, 2011, **50**, 5904–5908.

125 T. Tao, S. Lu, Y. Fan, W. Lei, S. Huang and Y. Chen, Anode improvement in rechargeable lithium-sulfur batteries, *Adv. Mater.*, 2017, **29**, 1700542.

126 L. F. Nazar, M. Cuisinier and Q. Pang, Lithium-sulfur batteries, *MRS Bull.*, 2014, **39**, 436–442.

127 A. Manthiram, Y. Fu, S. H. Chung, C. Zu and Y. S. Su, Rechargeable lithium-sulfur batteries, *Chem. Rev.*, 2014, **114**, 11751–11787.

128 R. Fang, S. Zhao, Z. Sun, D. W. Wang, H. M. Cheng and F. Li, More reliable lithium-sulfur batteries: Status, solutions and prospects, *Adv. Mater.*, 2017, **29**, 1606823.

129 D. Capková, M. Almáši, T. Kazda, O. Čech, N. Király, P. Čudek, A. S. Fedorková and V. Hornebecq, Metal-organic framework MIL-101(Fe)–NH$_2$ as an efficient host for sulphur storage in long-cycle Li–S batteries, *Electrochim. Acta*, 2020, **354**, 136640.

844 | *Inorg. Chem. Front.*, 2022, **9**, 827–844

This journal is © the Partner Organisations 2022